Coastal Engineering 184 (2023) 104346

Contents lists available at ScienceDirect

Coastal Engineering

journal homepage: www.elsevier.com/locate/coastaleng

The influence of vegetated marshes on wave transformation in sheltered estuaries

Rae Taylor-Burns [a,b,*], Kees Nederhoff [c], Jessica R. Lacy [d], Patrick L. Barnard [d]

[a] Contractor to the U.S. Geological Survey, Pacific Coastal and Marine Science Center, 2885 Mission Street, Santa Cruz, CA, 95060, USA
[b] University of California, Santa Cruz, 1156 High Street, Santa Cruz, CA 95064, USA
[c] Deltares USA, 8601 Georgia Avenue, Silver Spring, MD, 20910, USA
[d] U.S. Geological Survey, Pacific Coastal and Marine Science Center, 2885 Mission Street, Santa Cruz, CA, 95060, USA

ARTICLE INFO

Keywords:
Coastal protection
Waves
Marsh
San francisco bay
XBeach

ABSTRACT

Assessing the influence of marshes on mitigating flooding along estuarine shorelines under the pressures of sea level rise requires understanding wave transformation across the marsh. A numerical model was applied to investigate how vegetated marshes influence wave transformation. XBeach non-hydrostatic (XB-NH) was calibrated and validated with high frequency pressure data from the marsh at China Camp State Park in San Pablo Bay, California (USA). The model was used to examine how marsh and hydrodynamic characteristics change the potential for marshes to mitigate wave driven flooding. Model results demonstrate that hydrodynamics, vegetation, and marsh width influence wave transformation most, while marsh morphology parameters such as elevation and slope had least effect. Results suggest that in the range of settings explored here (incident wave heights ranging from 0.5 to 3 m and water levels ranging from current mean higher high water to 3 m above current mean higher high water), in comparison to wave propagation over an unvegetated mudflat, marsh vegetation reduces runup by a median of 40 cm and wave height by a median of 35 cm. Results illustrate how marshes can be strategically utilized to provide flood reduction benefits.

1. Introduction

Climate change is raising global sea levels and threatening coasts around the world with increased risk of flooding. Thermal expansion of seawater and melting of land-based ice is predicted to cause between 0.3 and 3 m of sea level rise (SLR) by 2 100 (DeConto and Pollard, 2016; Sweet et al., 2017, 2022; le Bars et al., 2017; Masson-Delmotte et al., 2021), which will significantly increase coastal flood risk (Vitousek et al., 2017; Taherkhani et al., 2020). In addition to SLR, coastal flooding is amplified by tides, storm-driven surge, waves, and river discharge (Barnard et al., 2019). Disproportionate population density in coastal areas further compounds this risk. More than 600 million people live in the coastal zone and that number is expected to increase to more than 1 billion by 2050 (Merkens et al., 2016). These factors combine to create hazard, exposure, and risk for coastal communities around the world. Coastal habitat such as coral reefs, mangrove forests and marshes can play a role in increasing resilience to storms and high water levels by buffering incoming waves and storm surge and stabilizing shorelines (Shepard et al., 2011; Ysebaert et al., 2011; Suzuki et al., 2012; Quataert et al., 2015; Narayan et al., 2016; Nowacki et al., 2017). Research suggests that wetlands reduced damage from Hurricane Sandy by $625 million (Narayan et al., 2017), coral reefs annually protect over 18,000 people (Storlazzi et al., 2019) and $1.8 billion dollars of infrastructure in the USA (Reguero et al., 2021), and mangroves provide $65 billion in flood protection benefits globally each year (Menéndez et al., 2020). Incorporating vegetation into levee systems on a global scale can reduce required levee height and result in cost savings on the order of $300 billion (van Zelst et al., 2021). Findings like these have caused a recent shift in scientific and management focus to nature-based shoreline protection (Powell et al., 2019).

Though coastal habitats have been shown to be effective in reducing flooding, projected sea level rise is anticipated to squeeze coastal habitat; for example, a morphological study of San Francisco Bay suggests that intertidal areas will drown with 21st century SLR (Elmilady et al., 2019), though this response depends on sediment supply, location, and morphology. A marsh with sufficient sediment supply may continue to accrete sediment on the marsh platform, raising its elevation gradually (Kirwan et al., 2010; Swanson et al., 2014). A marsh may also

* Corresponding author. 1156 High Street, Santa Cruz, CA 95064, USA.
E-mail address: rtaylorb@ucsc.edu (R. Taylor-Burns).

https://doi.org/10.1016/j.coastaleng.2023.104346
Received 1 March 2022; Received in revised form 24 March 2023; Accepted 26 May 2023
Available online 14 June 2023

respond to rising water levels with landward retreat of vegetation zones (Stralberg et al., 2011; Bigalbal et al., 2018), or lateral erosion and steepening of the marsh edge (Tommasini et al., 2019). Marshes that cannot keep up or migrate may lose vegetation density and transition to mudflat as the inundation periods begin to exceed the tolerance of marsh plants (Stralberg et al., 2011; Schile et al., 2014).

Wave energy on coasts dissipates through several processes. In the inner shelf and shoreface, dissipation occurs due to bottom friction (Putnam and Johson 1949), percolation (meaning transfer of energy into a permeable bottom; Putnam 1949; Shemdin et al., 1978), fluctuation in the bed level (Putnam and Johson 1949), and white capping (Hasselmann 1974); these processes can reduce wave energy significantly before waves ever begin to break. As waves enter the surf zone, turbulence due to depth-induced wave breaking is the primary driver of wave energy dissipation, though bottom friction also plays a role. There is great variation in energy loss due to breaking, depending on factors including surf zone morphology, infragravity energy, and breaker type (Wright and Short 1984). Finally, once waves reach the swash zone, energy loss occurs due to turbulence, bottom friction, and percolation (Stutz et al., 1998). Though swash, which is defined as the movement of water up the shore after the breaking of a wave, represents only a small fraction of the initial energy of waves, it can cause coastal morphology change and property damage.

Plants can reduce wave energy via work done by frictional drag. Vegetation-induced wave attenuation has been studied extensively, in field (Foster-Martinez et al., 2018; Garzon et al., 2019) and lab experiments (Bouma et al., 2013; Maza et al., 2015), as well as with empirical (Mendez and Losada, 2004) and physical models (Suzuki et al., 2012; Ma et al., 2013). The amount of drag plants provide depends on hydrodynamic conditions (Mendez and Losada, 2004; Callaghan et al., 2010; Foster-Martinez et al., 2018) and vegetation characteristics (Foster-Martinez et al., 2018). Dalrymple et al. (1984) developed an expression to describe energy dissipation of waves through a vegetated field, treating the vegetation elements as rigid cylinders, and subsequently that expression was modified for a random wave field by Mendez and Losada (2004), who also developed an analytical solution for shallow-water waves with a sloped water depth. The work of Mendez and Losada (2004) applies only to submerged plants, which are relatively short and stiff (such as marsh plants and some types of sea grass), and not to vegetation with low stiffness and high buoyancy (such as certain types of kelp), though it has been applied to vegetation with low stiffness.

The formulation developed by Mendez and Losada (2004) is the basis of wave attenuation in the XBeach model (van Rooijen et al., 2015). This formulation paired with the recent development of the XBeach non-hydrostatic mode, which, though computationally costly, is resolved for incident-band waves (XB-NH; de Ridder et al., 2020) enables a first look at the impact of vegetation on incident-band (i.e., short period or high frequency) driven wave runup, which is the sum of wave setup and swash (Miche 1951; Longuet-Higgins and Stewart 1963; Guza and Thornton 1981; Stockdon et al., 2006). Runup requires high frequency (wave resolved) data to observe, and in the past has been observed using time series imagery (Stockdon et al., 2006), which is challenging to collect. Though runup is a direct indicator of maximum coastal flooding, and is thus a key consideration in coastal planning, the interactions of wave runup (measured vertically) and vegetation are not well understood and have only recently begun to be studied (van Wesenbeeck et al., 2022). Previous studies have determined that wave height decay across vegetation fields depends on variables including water level, vegetation height, wave height, and frictional coefficient (Foster-Martinez et al., 2018; Garzon et al., 2019). However, other aspects of marsh morphology have not been considered, such as marsh platform elevation relative to tidal datum, mudflat and marsh edge slope, and marsh width. Furthermore, interactions between these variables have not been examined.

This study employs observational data from San Francisco Bay, California (USA), to calibrate and validate a model and establish that XB-NH can hindcast wave heights and periods in vegetation fields. Then, through experimental schematized simulations which vary hydrodynamic conditions, vegetation characteristics, and marsh morphology dimensions, this study examines the role of vegetation in reducing flooding potential. The analysis shows which characteristics of marshes control wave transformation and dynamic water levels, how these characteristics interact, and how the potential of marshes to reduce flooding may change with higher water levels.

2. Materials and methods

2.1. Study site

In the winter of 2014–2015, and the summer of 2016, Foster-Martinez et al. (2018) performed vegetation surveys and deployed pressure sensors along a transect in China Camp State Park (38.0095°, −122.4837°), in San Pablo Bay, in the northwest corner of San Francisco Bay. They characterized the marsh with four different vegetation zones: a low marsh, characterized by *Spartina foliosa*; a high marsh, characterized by *Salicornia pacifica*; and two transition zones, characterized by combinations of the two vegetation species. Vegetation surveys were conducted on January 23, 2015, and June 6, 2016, using 1-m quadrats to determine percent cover of each species and average and maximum canopy heights, which were determined by measuring the height of the tallest and a typical stem, and quarter-meter quadrats to determine stem count and stem diameter measurements. These values were measured for the high marsh and low marsh zones and interpolated linearly for the transition zones based on percent cover of high and low marsh vegetation. Pressure sensors were deployed on a 150 m transect, starting 35 m outside the marsh on the mudflat, and extending into the marsh, placed at the boundaries of the vegetation zones. These sensors collected data at either 6 or 8 Hz in bursts of measurements every 10 or 15 min. Bursts were 2048 measurements long, which is approximately 5 min at the given measurement frequencies. These data are publicly available (Lacy et al. 2017) and were utilized to calibrate and validate an XB-NH model. To convert total pressure to water depth, a constant water density was assumed and atmospheric pressure was temporally interpolated from measurements taken at the NOAA RCMC1 weather station, which is 11.5 km from the site, and subtracted from total pressure. A spectral analysis was used to determine variance density from pressure time series, and variance density (from which wave statistics such as peak wave period Tp, significant wave height Hs or Hm_0 can be calculated) was used to force calibration and validation model runs.

2.2. Model and data sources

XBeach (Roelvink et al., 2009) is a process-based model which simulates nearshore processes including wave transformation, wave-induced setup, over-wash, and inundation; in addition to information on water levels and wave heights, model outputs can include parameters such as flow and orbital velocity, bed shear stress, and stokes drift. XBeach was originally developed as a phase-averaged model that resolves amplitude variation on the wave group scale (surfbeat) but does not resolve individual waves as in a Boussinesq model. Recently, a non-hydrostatic mode (XB-NH) was developed for XBeach (de Ridder et al., 2020), which is similar to a depth-averaged version of the SWASH model (Zijlema et al., 2011; Smit et al., 2013) and is able to fully resolve incident-band waves. Resolution of incident-band waves, though computationally costly, is necessary to determine swash on relatively steep slopes and is thus necessary to investigate runup (as determined by the last wet grid cell), and potential overtopping on levees. Runup and overtopping in the non-hydrostatic mode have been validated using several separate datasets from sandy beaches. Results show that incident-band driven runup height is predicted with good accuracy and a maximum deviation of 15% (Roelvink et al., 2018). A reduced

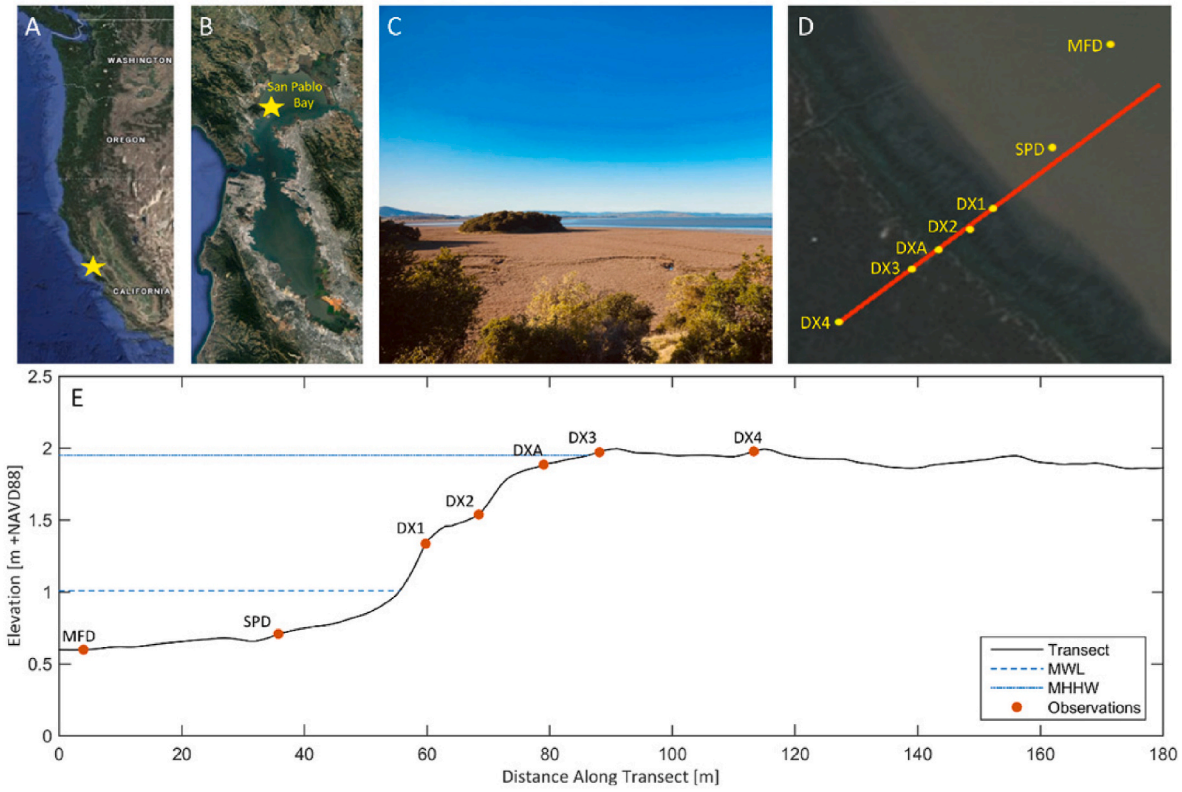

Fig. 1. Location (A and B; base-map layer from Google Earth) and view (C; photograph taken by R. Taylor-Burns) of the study site, and depiction of the transect deployed in 2016 by Lacy et al. (2017); D and E). MDF is the offshore site, SPD marks the beginning of the low marsh, DX1 marks the beginning of the first transition zone, DX2 marks the beginning of the second transition zone, and DXA – DX4 are all on the high marsh.

two-layer non-hydrostatic formulation is included that allows for a more accurate description of the frequency dispersion in relatively deeper water. Relative depth (KD) determines whether waves are in deep water (waves do not interact with the bottom, $KD > \pi$) or shallow water (waves interact with the bottom, $KD < \pi/10$), and is based on water depth and wavelength. de Ridder et al., 2020 showed good performance up to a relative depth of 3. XB-NH allows for the inclusion of the effect of vegetation within the model via vegetation parameters including stem density, frictional drag coefficient, stem height, and stem diameter (van Rooijen et al., 2015; van Rooijen et al., 2016).

In this study, XB-NH was applied in one-dimensional mode. This approach assumes that wave forcing is shore-normal and neglects lateral flow, assumptions which were also made in the analysis by Foster--Martinez et al. (2018). This approach also neglects tidal channels and creeks, which facilitate drainage of water on the marsh. Model boundary conditions were determined by obtaining wave statistics from every burst at the offshore observation station, MFD (Fig. 1). Bathymetry was determined from a 2 m digital elevation model (DEM), which was collected aerially with Light Detection and Ranging (LiDAR) (Danielson et al., 2016). Discrepancies between elevations at the study sites in the DEM and elevations reported by Lacy et al. 2017 ranged from 0 to 20 cm, with largest discrepancies in the high marsh zone. These discrepancies are likely due to LiDAR overestimating elevation in dense vegetation. A vegetation-corrected DEM (only available at elevations above −1 m NAVD88) was also tested (Buffington and Thorne 2018), but it also had discrepancies and had lower spatial resolution (5 m) and thus was not used. To correct for vertical discrepancies between field observations and the 2 m DEM, a linear interpolation of the discrepancies was created and subtracted from the DEM.

Variable grid spacing was used, with a minimum of 30 grid points per wavelength and the total number of grid points ranging from 1,500 to 19,000. Sensitivity analyses show that the model results converge at this resolution. A Manning's friction formulation was used for mudflat friction. The equilibrium bound long wave, which is energy that fluctuates at the same frequency as the wave group but 180° out of phase, was not imposed in the calibration or validation as this saved significant computational time and did not impact model results. In contrast to open-coast conditions, offshore spectra in this sheltered environment do not show components of bound long waves in the variance density spectrum. We hypothesize that this is related to the relatively young age of the sea-state in combination with steep slope compared to wave period in San Pablo Bay. To determine wave statistics from water level time series, a Guza filter (Guza et al., 1984) was used to separate incoming and outgoing wave energy. A fast Fourier transform was used to determine wave spectra from water level time series. Significant wave height and peak period were determined from wave spectra. The last wet grid cell was utilized to determine a runup time series and the 98th percentile of this time series was utilized to determine R2%, or the runup value which is exceeded by 2% of waves.

2.3. Calibration and validation

Bursts for which the significant wave height was greater than 5 cm at the offshore station (MFD), and for which ratio of wave group velocity to phase velocity (c_g/c_p, or N) was less than 0.85 at the offshore station, were selected for calibration and validation in order enable us to model meaningful decay of wind waves with deep water boundary conditions. Few bursts during the summer deployment met these conditions, so the model was developed using winter measurements, with the calibration dataset from January 15–25, 2015 (n = 257), and the validation dataset from December 18–28, 2014 (n = 88). For all bursts, the relative depth (KD) was less than 1.5, and the ratio of wave height to water depth was less than 1/3.

The vegetation module of XB-NH was utilized to account for wave-

Table 1
Vegetation parameters used in the model calibration. Values for stem diameter, vegetation height, and stems/m^2 for the low and high marsh are taken from the field surveys done by Foster-Martinez et al. (2018). Stem diameter and vegetation height for the transition zones are linearly interpolated from the high and low marsh, based on proportional vegetation cover of the two main vegetation species. Stem density for the transition zones is determined by back-calculating from the $N \times B_v$ values listed in Table 1 of Foster-Martinez et al. (2018). Values of drag coefficient (Cd) are the mean of values calculated by Foster-Martinez et al. (2018) from the winter deployment, except for the low marsh Cd, which is from the summer deployment.

Marsh zone	Species	Stem diameter (m)	Vegetation height (m)	Stems/m^2	Cd
Low marsh	*Spartina foliosa*	0.0027	0.16	312	0.34
Transition zone 1	20% *S. foliosa*, 15% *S. pacifica*	0.0024	0.186	5 583	0.43
Transition zone 2	5% *S.foliosa*, 55% *S. pacifica*	0.00205	0.215	23,562	0.56
High marsh	*Salicornia pacifica*	0.002	0.22	44,000	0.93

vegetation interactions within the marsh (van Rooijen et al., 2015). Stem height, diameter, and density for each of the four vegetation zones were taken from the vegetation surveys done by Foster-Martinez et al. (2018). That study calculated drag coefficients, Cd, for the 4 vegetation zones in winter and summer and found, progressing from the bay to the marsh, that the mean and standard deviation of Cd across the four vegetation zones and spanning the full range of water level conditions to be [9.85 ± 19.23, 0.44 ± 0.33, 0.56 ± 0.25, 0.93 ± 0.53] for winter and [0.34 ± 0.41, 0.56 ± 0.19, 0.41 ± 0.10] for summer (there was only one transition zone during the summer deployment). The Cd for the low marsh in winter is very high due to low vegetation frontal area at that time, caused by seasonal loss of leaves (see Fig. 4 in Foster-Martinez et al. (2018) for a visual), but similar wave attenuation to the summer months. Foster-Martinez et al. (2018) discusses possible mechanisms for similar attenuation despite seasonal changes in marsh plants. Additionally, uncertainty for Cd in the low marsh during winter is very high. Because that value is anomalously high, with high uncertainty, and inconsistent with other values reported in the literature, the summer Cd value for the low marsh was used, such that the values of Cd we used across the four vegetation zones were [0.34, 0.44, 0.56, 0.93], respectively. Vegetation parameters for calibration are shown in Table 1.

Model results were assessed by comparing modeled and measured wave heights and wave periods. Predictive skill was determined by calculating relative bias (RB), scatter index (SCI), and mean absolute error (MAE), using equations (1)–(3), where m is the measured value, c is the calculated value, and n is the number of observations. For model calibration, values of Cd were varied for each of the four vegetation zones, several DEMs were tested, and the Manning's coefficient of the mudflat and maximum breaking steepness of waves were varied as well.

$$\textit{Relative bias}\ (RB) = \overline{(c-m)}\Big/_{|\overline{m}|} \tag{1}$$

$$\textit{Scatter index}\ (SCI) = \sqrt{\overline{(c-m)^2}}\Big/_{|\overline{m}|} \tag{2}$$

$$\textit{Mean absolute error}\ (MAE) = \sum|c_i - m_i|\Big/_{n} \tag{3}$$

Previous research shows that Cd varies with Reynolds or Keulegan-Carpenter numbers (Mendez and Losada, 2004; Pinsky et al., 2013; Foster-Martinez et al., 2018) and that as turbulence increases, Cd decreases. The field campaign carried out by Foster-Martinez et al. (2018) observed a limited range of Reynolds numbers (Re < 600), so we used a constant Cd across all calibration and validation bursts. The Cd was treated as a bulk drag coefficient, or an empirical coefficient appropriate for the whole vegetation field. It was determined by the mean value from the range of observed hydrodynamic conditions and was not time-varying, following the approach of van Rooijen et al. (2016). Like van Rooijen et al. (2016), model-data agreement in this study was found to have relatively low sensitivity to small changes in values of Cd. Calibration and validation skill scores are shown in Fig. 2. See Fig. S1 for a detailed look at several individual bursts.

Calibration results showed that the model was relatively insensitive to Manning's friction coefficient of the mudflat and the maximum steepness of waves before breaking. Model sensitivity to bathymetry was similar to sensitivity to changes in vegetation drag coefficient ranging up to one standard deviation, or a factor of about two (Table S1). Given that maximum steepness and Manning's coefficient are not strong controls on the model and given the uncertainty in the 2 m DEM, the default

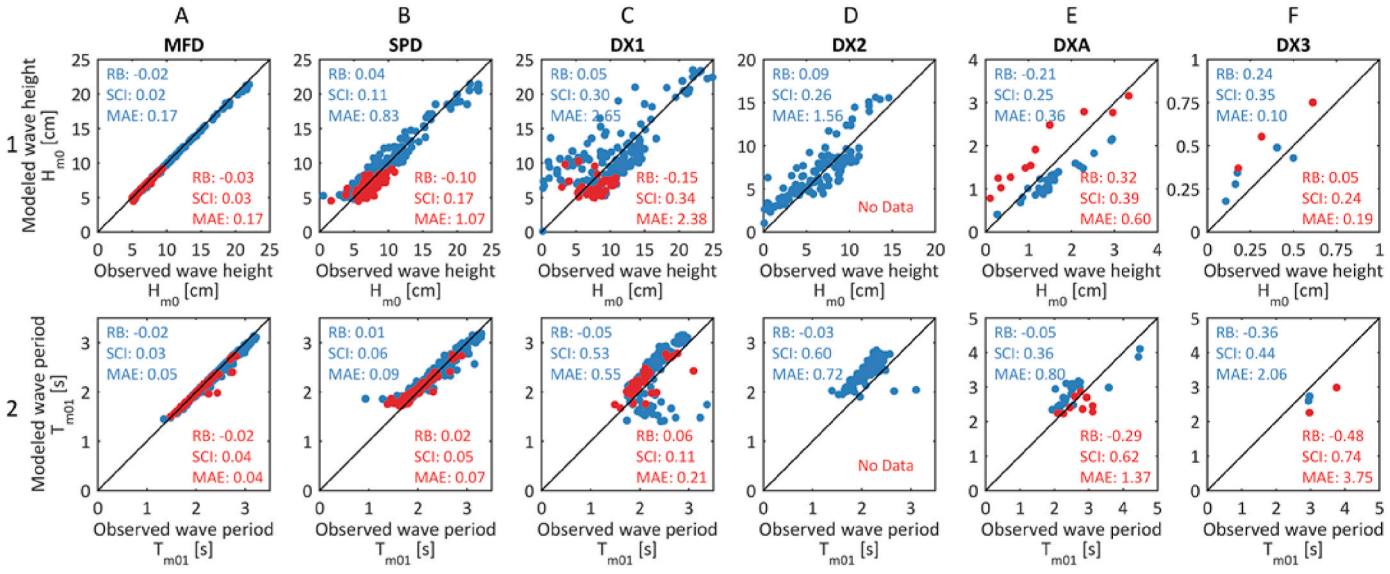

Fig. 2. Results from model calibration (red) and validation (blue), showing wave height (row 1) and wave period (row 2). Columns A through E show model-data agreement at the six offshore observation locations at China Camp State Park, MFD, SPD, DX1, DX2, DXA, and DX3. Locations of these points can be seen in Fig. 1. Skill scores correspond to relative bias, scatter, and mean absolute error. No calibration data are shown in column D because data were not collected at DX2 during the calibration period.

Table 2
A summary of marsh parameters observed in a 2013 regional survey done by Takekawa et al. (2013), followed by a summary of vegetation parameters found in existing literature.

Marsh tidal data					Survey observations (m NAVD88)	
Mean sea level (MSL)					0.99–1.21[a]	
Mean high water (MHW)					1.70–1.92	
Mean higher high water (MHHW)					1.85–2.09	
Mean marsh elevation					1.4–2.1 m [b]	
Marsh vegetation zones					**Survey observations (m relative to MSL)**	
Typical mudflat elevation					< +0.2	
Typical low marsh elevation					+0.2–0.45, mostly Spartina spp	
Typical mid marsh elevation					+0.45–0.7	
Typical high marsh elevation					> +0.7, mostly Salicornia pacifica	
Species	Stem density (stems/m^2)	Stem diameter (m)	Vegetation height (m)	Cd	Location	Citation
Salicornia pacifica	44000	0.002–0.0034	0.22–0.25	0.41–0.93	SF Bay	Foster-Martinez et al., (2018)
Spartina foliosa	312–440	0.0027–0.0047	0.16–0.48	0.34	SF Bay	Foster-Martinez et al., (2018)
Various marsh species	500 (model)	0.007 (model)	1.5 (model)	0.01–10 (mean = 2.6)	various	Pinsky et al., (2013)
Spartina alterniflora and *Spartina patens*	100–500	0.007	1.5		North Carolina	Gittman et al., (2014)
Spartina foliosa	284		0.94		Tijuana Estuary	Ward et al., (2003)
Spartina foliosa	270				Tijuana Estuary	Desmond et al., (1999)
Salicornia pacifica			0.15–0.35		SF Bay	Woo and Takekawa (2012)
Salicornia europaea	1 200–10000		0.05–0.2		Rhode Island	Ellison (1987)

[a] 10 of the 12 surveyed marshes had mean sea levels between 0.99 and 1.07 m NAVD88.
[b] 11 of the 12 surveyed marshes had mean marsh elevations between 1.6 and 2.1 m NAVD88.

value for maximum wave steepness was used (0.4), a standard Manning's friction was used for the mudflat (0.018 s/m$^{1/3}$, Shen et al., 2006; Fernandes et al., 2000; Chow 1959) and the vegetation drag coefficients calculated by Foster-Martinez et al. (2018) based on field observations were used.

In many bursts, both observed and modeled wave spectra have a peak at very low frequencies, resulting in both modeled and observed wave periods of up to 400 s. We hypothesize this is due to the length of bursts at which data were collected and the method of spectral analysis. However, long period infragravity waves (Talke and Stacey 2003) or basin and sub-basin oscillation motions such as seiching (Kimmerer 2004) could also be at play. The focus of this analysis is on local wind waves and therefore these bursts have been excluded. The calibration process also revealed that the model does not simulate propagation of waves less than 1 mm, because XB-NH does not model capillary waves. Thus, bursts in which wave transformation over the transect resulted in peak wave periods greater than 20 s and significant wave heights less than 1 mm were excluded from the plots and skill scores shown in Fig. 2, which is why there are many more data points at the offshore boundary than on the marsh platform.

The model hindcasts wave height and wave period, establishing that XB-NH effectively models wave transformation in vegetation fields. There is an over-prediction of wave period in the transition zones of the marsh (Fig. 2, 2C, 2D), and an underprediction of wave period in the high marsh (2 F). Wave heights during the calibration and validation phase at DX1 have negative and positive bias, respectively (Fig. 2, 1F). However, the observed wave heights are small (<4 cm), and thus the biases could be due to changes in the bathymetry between the calibration and validation time periods, which were a month apart.

2.4. Schematized model setup

Having established that XBeach, a process-based model, is able to hindcast wave transformation in vegetation, we changed physical parameters in the model to explore the full range of possibilities that have been observed and modeled in our study region and similar study regions, including variations in vegetation, marsh morphology, and hydrodynamics, with a goal of creating idealized simulations that are applicable to other locations in San Francisco Bay as well as other estuaries. The model settings from calibration and validation were used and physical parameters were varied, including Cd, following the approach taken by Quataert et al. (2015), Best et al. (2018), and Harris et al. (2018). Takekawa et al. (2013) performed an extensive regional survey of San Francisco Bay marshes, and observations from this survey (Table 2) were used to determine physical parameters of schematized model transects. Multiple vegetation surveys were used (Table 2) to determine typical values and ranges for stem height, diameter, density, and values of Cd.

Table 3
A summary of vegetation parameters used in the schematized experimental model runs, followed by a summary of the range of parameters that were varied in the schematized experimental runs. In the bottom half of the table, an asterisk denotes variables that were covaried in all simulations.

Marsh Zone	Stems/m^2	Stem height [cm]	Stem diameter [mm]	Cd
Low	400	15	3	0.3
Transition	20,200	20	2.5	0.6
High	40,000	25	2	0.9

Parameter	Range	Source
*Water level**	[1.85, 2.5, 3, 4, 5] m NAVD88	Nederhoff et al., (2021)
Wave height	[0.5, **1**, 1.5, 2, 3] m	O'Neill et al., 2017
Wave steepness	[0.025, 0.035, **0.04**, 0.045, 0.055]	Zhao and Li (2019)
Vegetation density	[0, 0.5, **1**, 1.5, 2] × values listed above	Foster-Martinez et al., (2018)
*Cd, Frictional drag coefficient of vegetation**	[0.1, 0.5, 1, 2, 10] × values listed above	Foster-Martinez et al., (2018), Pinsky et al., (2013)
Minimum elevation of vegetation	[0, +10, + **20**, +30 + 40] cm relative to MSL	Takekawa et al., (2013)
Mudflat slope	[1:100, 1:200, **1:300**, 1:400 1:500]	Danielson et al., (2016)
Low marsh slope	[1:10, 1:20, **1:30**, 1:40, 1:50]	Danielson et al., (2016)
Marsh platform elevation	[-25, −15, **-5**, +5, +15] cm relative to MHHW	Takekawa et al., (2013)
Marsh platform width	[50, 100, 250, 500, 750, **1 000**] m	Danielson et al., (2016)

Schematized transects included, from bay to marsh, a sloped mudflat, a sloped marsh edge, a flat marsh top, and an unvegetated levee. The levee was included to ensure there is no flow out the back of the transect, with a slope of 1/10 and a height of +10 m NAVD88. The seaward boundary of each transect had a depth of −5 m NAVD88, thus resulting in ~500–2 500 m of mudflat leading up to the vegetated marsh, depending on the mudflat slope. The transitions between the first three zones were smoothed with a spline interpolation. Mean sea level (MSL) was set at 1 m (NAVD88), and mean higher high water (MHHW) was set at 1.85 m (NAVD88) (Takekawa et al., 2013). The low marsh vegetation zone was set between +0.2 and + 0.45 m MSL, the transition zone was set between elevations of +0.45 and + 0.7 m MSL, and the high marsh was set above +0.7 m MSL (Takekawa et al., 2013). Regional surveys show that *S. pacifica* is dominant in the high marsh, and *S. foliosa* is dominant in the low marsh, and that these two species are dominant and nearly equally abundant in the transition zone (Takekawa et al., 2013). Foster-Martinez et al. (2018) also showed that drag coefficients are strongly dependent on the vegetation survey methods; thus, in the schematized models we used a range of vegetation density and frictional values centered on those measured (stem diameter, stem height and stem density, for which we picked values in the middle of the ranges reported) and calculated (Cd, which we rounded to one significant figure, as shown in Table 3) by Foster-Martinez et al. (2018). These vegetation parameters are consistent with studies of similar vegetation from other regions.

A 30-year hindcast by O'Neill et al. (2017) suggested that the largest waves formed (99.9th percentile; i.e., exceeded 9 h per year) in San Francisco Bay during the time period 1975 and 2004 reached significant wave heights of 1.38–1.93 m, depending on basin subregion. Similarly, field observations in the shallows of San Pablo Bay showed that significant wave height frequently surpasses 0.5 m in summer months, and can reach up to 0.8 m during winter storms (Lacy and MacVean 2016). These extreme wave heights occur in the main channels of the bay, where water depth is greatest, but can propagate toward marshes in the bay shallows; the same field observations show that wave height decays by 50% over 6.5 km of mudflat. A 70-year water level hindcast by Nederhoff et al. (2021) suggested that storm-driven water levels in San Francisco Bay can exceed 1.2 m above predicted tides. Beyond high water levels driven by storm conditions, sea level rise is predicted to cause relative elevation of marshes to decrease by between 0.4 and 1.3 m in San Francisco Bay by the end of the century under a moderate emissions scenario (Swanson et al., 2014). Thus, by the end of the century, San Francisco Bay marshes could be exposed to up to 2.5 m of additional water level during storms. Higher water levels in estuaries will increase depth and fetch, enabling larger waves to form (Lacy and MacVean 2016; Karimpour et al., 2017). For example, previous research suggested that 1 m of sea level rise in San Francisco Bay will result in up to 0.4 m greater wave heights during a 100 year storm (O'Neill et al., 2017), though this depends on bay sedimentation rates (Ranasinghe et al., 2013). To account for daily and storm wave conditions in San Francisco Bay, as well as estuaries with greater fetch, we simulated wave heights ranging from typical present day conditions (Lacy and MacVean 2016) to 1.5–2 × present day modeled extreme San Francisco Bay wave height (O'Neill et al., 2017). Thus, in some simulations, waves are already breaking by the time they reach the marsh, resulting in greater dissipation over the mudflat as compared to dissipation over vegetation. Experimental models were forced with a JONSWAP spectrum (Hasselmann et al., 1973). To account for storm water levels as well as higher water levels due to rising sea levels, water levels from present day MHHW (1.85 m NAVD88) to 3.15 m above present day MHHW (5 m NAVD88) were used as boundary conditions. Existing marshes tend to have marsh platform with elevations within 20 cm of MHHW, thus this study simulates marshes with 0.05–3.2 m of inundation. See Table 3 for

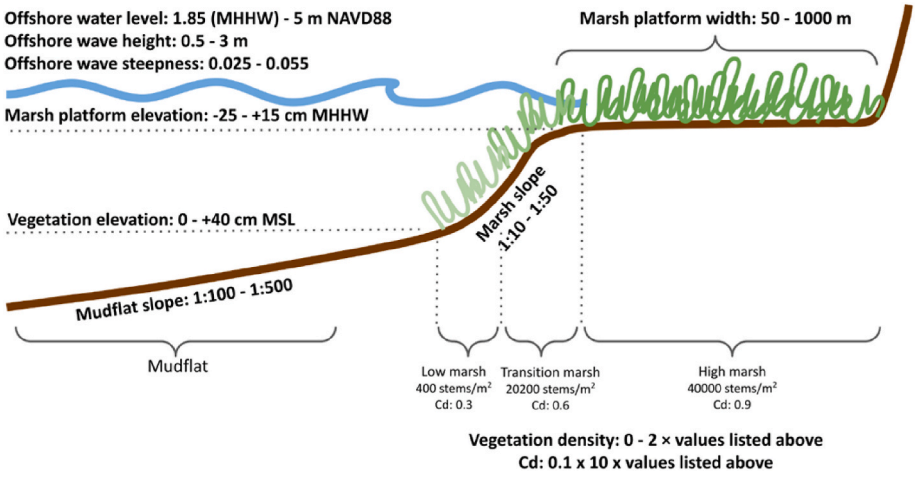

Fig. 3. Depiction of the schematized transect. Bolded text identifies variables that were changed in the schematized model runs.

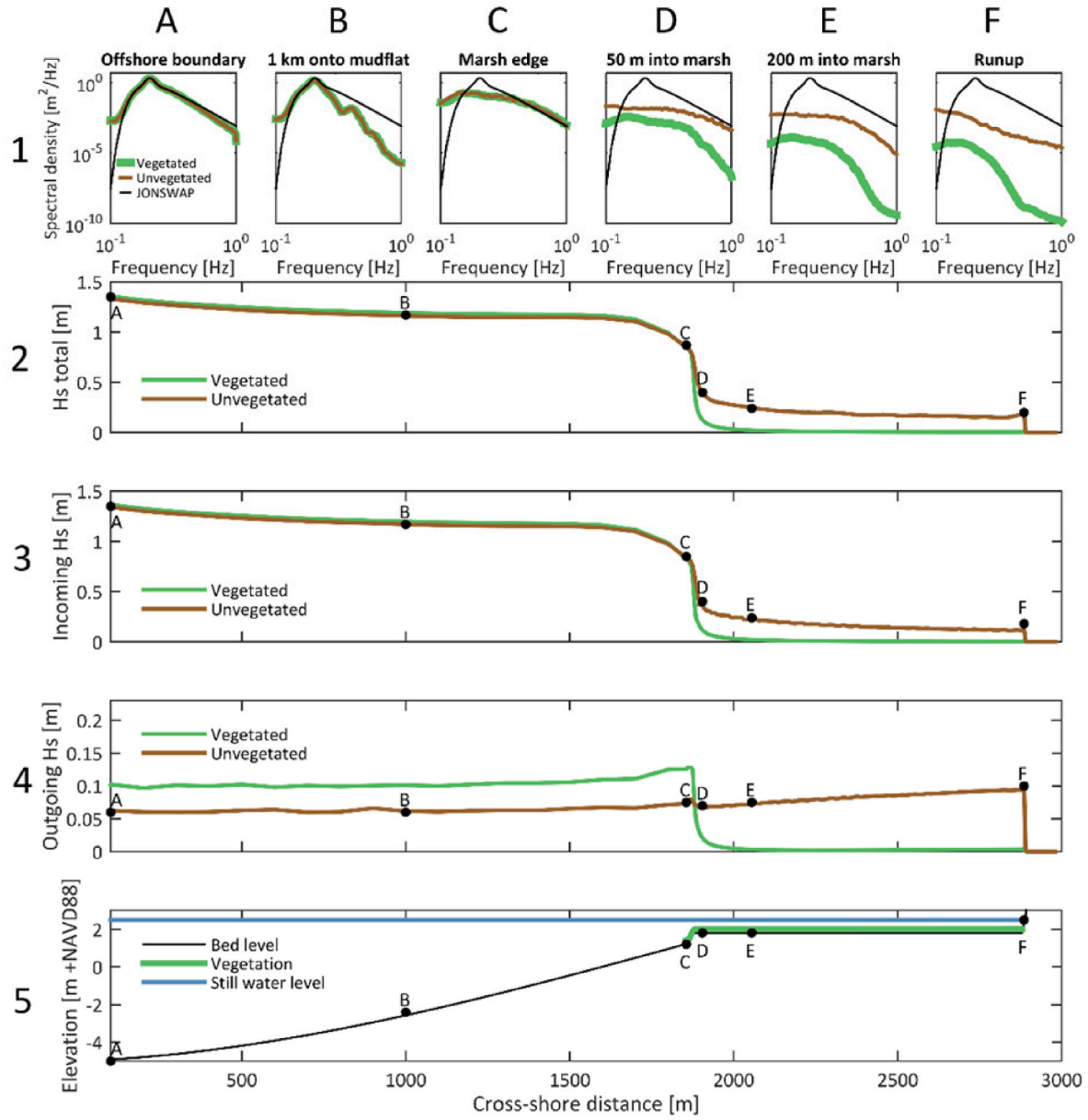

Fig. 4. The effects of vegetation on spectral density of wave energy and on wave height. Green lines show model results from a transect with a vegetated marsh and brown lines show results from a transect with an unvegetated marsh. Row 1 row shows, from left to right, spectral density at the offshore boundary (1 A), 1 km onto the mudflat (1 B), at the edge of the marsh (+1.2 m NAVD88, 1C), 50 m into the marsh (1D), 200 m into the marsh (1 E), and of the runup signal (1 F), with the y-axis plotted in log scale. Black lines in row 1 indicate idealized JONSWAP spectra determined by wave statistics used at the offshore boundary, which diverge from model results at low frequencies due to wave-wave interactions. The middle three rows show, from top to bottom, total significant wave height (row 2), incoming wave height (row 3), and outgoing, or reflected, wave height (row 4). The bottom row (row 5) shows transect bathymetry in black, vegetation location in green, and mean water level in blue. Bathymetry and water level are identical for the vegetated and unvegetated model. Black labeled dots on the bottom four plots show locations of the spectra in the top row (runup location is variable and thus approximate). Models were forced with wave heights of 1.5 m and steepness of 0.04 (peak period of 4.9 s), and water level was 2.5 m NAVD88 (or 0.65 m of marsh inundation). Drag coefficient (Cd) was 10% of China Camp observations.

more information on experimental simulation boundary conditions.

Previous studies with explicit vegetation representation show that Cd can vary widely between sites and under different hydrodynamic conditions (Pinsky et al., 2013; Foster-Martinez et al., 2018). Pinsky et al. (2013) found that drag coefficients ranged from 0.5 to 30 for similar hydrodynamic conditions, illustrating that Cd is a highly variable and uncertain parameter. Numerous studies quantify relationships between Cd and Re in marsh vegetation, but these relationships vary widely and do not extend beyond $Re > 10^3$. Because established relationships between Re and Cd do not extend beyond $Re > 10^3$, in higher Re simulations Cd values are an approximation. To account for this uncertainty in Cd, as well as variations in vegetation density and stem diameter, which also have direct effects on energy attenuation formulation developed by Mendez and Losada (2004), in this study we used a three order of magnitude range of drag coefficients, centered on the average of the four-week study period in China Camp, which spanned a variety of tidal and wave conditions.

Table 3 and Fig. 3 illustrate the schematized model settings that were used. In the first round of simulations, for each variation in schematized model settings shown in Table 3 (base case values are bolded in column 2 of Table 3), a range of water levels and frictional coefficients were used (shown by asterisks in column 1 of Table 3) to create a suite of multi-dimensional model runs and investigate how each parameter impacts the ability of marshes to transform waves and reduce potential flooding.

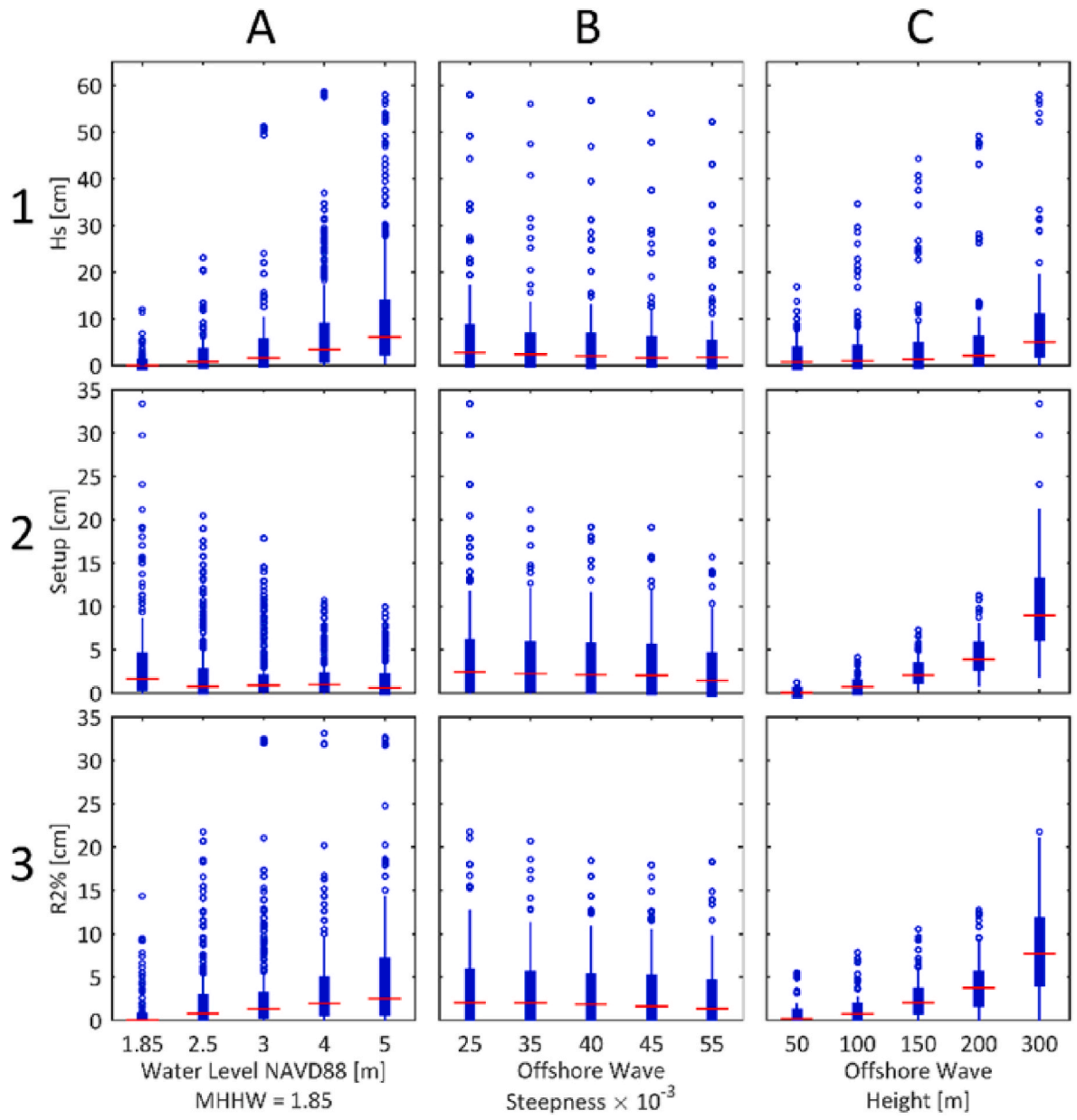

Fig. 5. Box plots showing changes in wave transformation across the marsh. Wave transformation metrics are on the y axis of all box plots, including: wave height 100 m into the high marsh (Hs, row 1), wave induced setup 100 m into the high marsh (row 2), and R2% (row 3). Characteristics of hydrodynamic conditions are on the x axis of all box plots, including water level (column A), offshore wave steepness (column B), offshore wave height (column C), with each box representing results from all simulations in which the specified hydrodynamic condition has the same setting. Red lines indicate medians, blue rectangles indicate the interquartile range, and blue dots indicate outliers. There are many positive outliers that are caused by coincidence of high water levels and low drag coefficient (Cd). Water level and wave height are the strongest controls on wave transformation.

Each model was run with vegetation present and with vegetation completely removed, to separate the influence of vegetation and the influence of bathymetry. In the unvegetated models, the Manning's friction coefficient determined from calibration and used on the mudflat was applied across the entire transect. This process consisted of 1 650 XB-NH simulations. Results can be seen in Section 3.2 and were utilized to identify parameters most important in controlling wave transformation.

Based on results from the first round of simulations, a second round of simulations was subsequently run. In the second round of simulations, the key parameters identified in the first round of simulations (italicized in column 1 of Table 3) were all covaried, creating a complete set of every combination of the key drivers of wave transformation in the ranges identified in Table 3 and Fig. 3, both with vegetation present and with vegetation removed from the transect. This process consisted of 3 750 XB-NH simulations and results can be seen in Section 3.3.

All runs were at least 1,000 waves long (based on peak period) plus 60 min of spin-up (400–1,500 waves, depending on period) to reach stationarity of the wave setup, which were not used for analysis. Model results were post-processed to obtain significant wave height 100 m into the high marsh (Hs), average wave-induced setup 100 m into the high marsh (setup), and the 98th percentile runup value (R2%). Hs was calculated spectrally using functions available on Open Earth Tools, which is a repository for free and open-source code for a variety of topics related to delta and coastal areas (https://publicwiki.deltares.nl/display/OET/OpenEarth); setup was calculated as the mean water level 100 m into the marsh relative to the offshore water level (i.e., at the offshore edge of the transect, which is between 500 and 2 500 m offshore

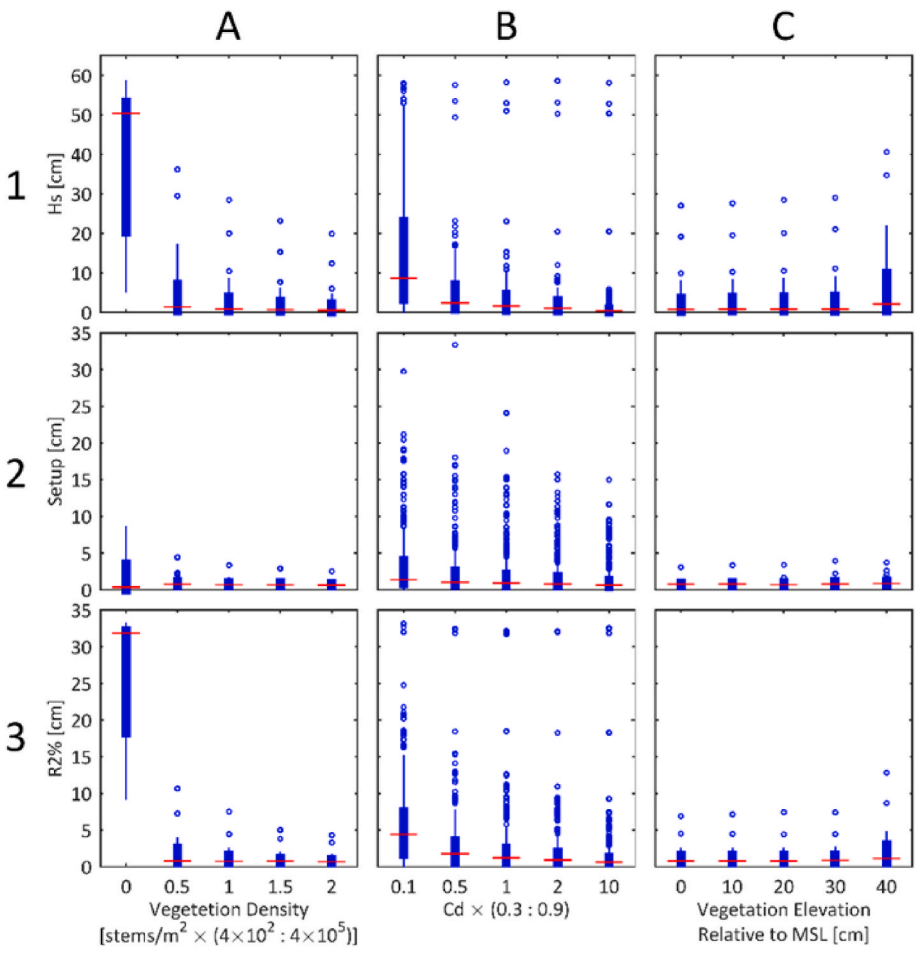

Fig. 6. Box plots showing changes in wave transformation across the marsh. Wave transformation metrics are on the y axis of all box plots, including: wave height 100 m into the high marsh (Hs, row 1), wave induced setup 100 m into the high marsh (row 2), R2% (row 3). Characteristics of vegetation are on the x axis of all box plots, including vegetation density (column A), vegetation frictional drag coefficient (Cd, column B), and minimum vegetation elevation (column C), with each box representing results from all simulations in which the specified vegetation condition has the same setting. Red lines indicate medians, blue rectangles indicate the interquartile range, and blue dots indicate outliers. There are many positive outliers that are caused by coincidence of high water levels and low Cd. Vegetation density and Cd are the strongest controls on wave transformation.

from marsh edge, depending on mudflat slope); runup was also calculated relative to the offshore water level. Thus, runup is determined by the total water level at the last wet grid cell (TWL) minus the still water level at the offshore boundary (SWL) and includes both swash and setup. In the shortest marsh settings (50 m of vegetation), Hs and setup were measured at the last vegetated grid cell.

3. Results

3.1. Wave transformation due to vegetation

To examine and isolate the impact of vegetation on wave transformation, spectral analyses of the incoming water level and subsequent computed wave energy and height from the schematized experimental model runs were completed; an example of this is shown in Fig. 4. Results show that a large proportion of wave decay due to vegetation happens across a short horizontal distance, with the majority of wave energy dissipation due to vegetation occurring in as little as 50 m into the marsh vegetation (1D), which is approximately 30 m into the high marsh. This decay in wave height (row 2) and wave energy (1D and 1E) is due to reflection of wave energy by vegetation, which is shown by the peak in the outgoing wave height at that point on the transect (row 3), and to frictional drag. Additionally, wave spectral energy analysis reveals that vegetation reduces relatively higher frequency energy first, and as waves travel up the transect through the marsh vegetation, spectral energy is transferred toward lower frequencies (1D, 1E and 1F).

3.2. Effects of marsh and hydrodynamic settings

The capacity of a marsh to reduce potential flooding increases with increasing vegetation density, Cd, and wave steepness and decreases with increasing minimum elevation of vegetation, water level, and wave height (Figs. 5–7). Generally, there are many positive outliers, which signify that when high water levels and low friction coefficients coincide, the potential of marshes to reduce waves and flooding decreases. Marsh width, vegetation friction, water level, and wave height conditions are the strongest controls on wave transformation.

3.2.1. Hydrodynamic conditions

Increasing water level (Fig. 5, column A) results in an increase in Hs and runup. At higher water levels, bathymetric effects are reduced, mudflat friction decreases per the Manning friction formulation, and the relative height of vegetation decreases, thus reducing frictional drag by marsh plants. Increasing the steepness of offshore waves (column B) decreases the wave period, thus decreasing the wave power. This causes a decrease in Hs, setup and runup. In the range of conditions studied here, wave height has a stronger effect on wave transformation metrics than wave steepness. Increasing wave height (column C) causes an increase in Hs, setup and runup as expected based on prior work (Guza and Thornton 1981, 1982; Stockdon et al., 2006).

3.2.2. Vegetation characteristics

Increasing vegetation density (Fig. 6, column A) and increasing Cd (column B) cause similar impacts on wave transformation and flood reduction, resulting in decreased Hs, setup, and runup by increasing the short-wave dissipation due to vegetation. Increasing the minimum

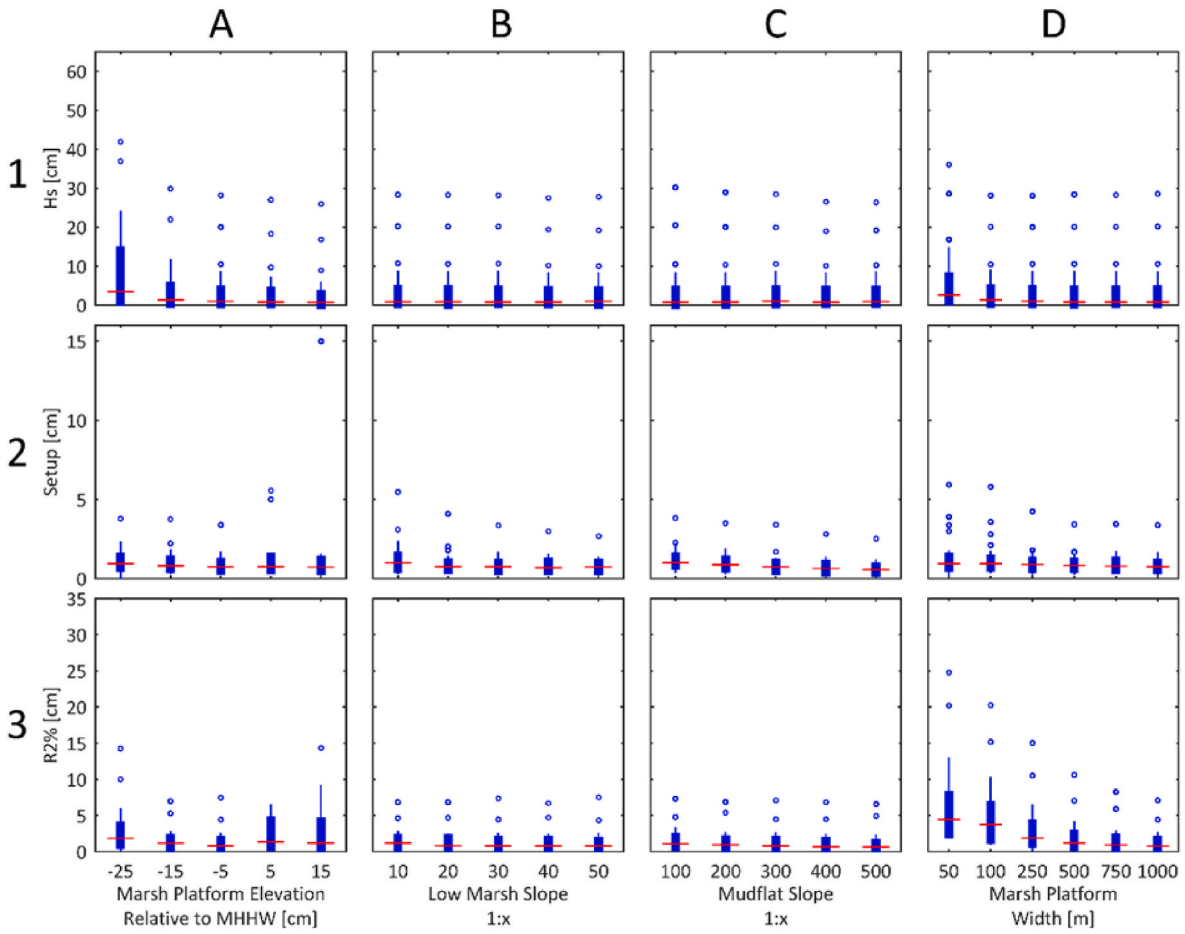

Fig. 7. Box plots showing changes in wave transformation across the marsh. Wave transformation metrics are on the y axis of all box plots, including: wave height 100 m into the high marsh (Hs, row 1), wave induced setup 100 m into the high marsh (row 2), and R2% (row 3). Characteristics of marsh morphology are on the x axis of all box plots, including marsh platform elevation (column A), low mash slope (column B), mudflat slope (column C), and marsh platform width (column D), with each box representing results from all simulations in which the specified morphology condition has the same setting. In the shortest marsh setting, Hs and setup were measured at the last vegetated grid cell. Red lines indicate medians, blue rectangles indicate the interquartile range, and blue dots indicate outliers. There are many positive outliers that are caused by coincidence of high water levels and low drag coefficient (Cd). Marsh width is the strongest control on wave transformation.

elevation of vegetation (column C) causes a greater proportion of the transect to be unvegetated, resulting in waves traveling over more mudflat and a narrower vegetation field. Thus, increasing the vegetation elevation decreases dissipation due to vegetation. This causes an increase in Hs, setup, and runup. The highest setting of vegetation elevation eliminates the high marsh zone completely, meaning that only low and transition marsh zones are present. This setting results in the greatest change of the wave reduction metrics suggesting that minimum elevation of vegetation has little impact on wave transformation until the high marsh zone is completely lost.

3.2.3. *Marsh morphology*

The marsh morphology settings include marsh platform elevation, low marsh slope, mudflat slope, and marsh platform width. These settings had the weakest influence on wave transformation with marsh platform width providing the greatest variation, particularly in runup. Increasing the marsh platform width (Fig. 7, column D) decreases runup because waves must travel across more vegetation before hitting the levee and causing runup. Thus, waves are dissipated more as they travel across the marsh platform in wider marshes, causing less runup at the levee.

3.3. *Key drivers of wave transformation*

The cumulative sum of the difference in medians of Hs, setup, and runup across the range of model settings was calculated (Fig. 8). For example, the top bar shows the difference in median Hs (blue), setup (orange), and runup (red) between the highest and lowest offshore Hs simulated. Variables which produced a cumulative sum of greater than 5 cm were identified as the most important factors that influence the impact of marshes on wave transformation. These include Hs, Cd, water level, and marsh width.

We ran a subsequent set of simulations using the same settings described in Table 3 in which five different factors were covaried (wave height, water level, Cd, marsh width, and wave steepness) to identify combinations of settings that resulted in extreme results, and to further explore the key drivers of wave transformation in marsh ecosystems. Wave steepness was included to provide a more complex look at wave and vegetation dynamics and to allow for multiple settings for each run. All runs were done with and without vegetation present. An overview of results from the second round of simulations is shown in Fig. 9.

Across the range of conditions explored here, which represent 5^5 simulations with settings described by italicized entries in Table 3, vegetation reduces significant wave height 100 m into the marsh by a median of 35 cm (Fig. 9, 1B) and 94% (1C). The middle 95% of significant wave height reduction due to vegetation (cm) falls in the range [1, 157]. Vegetation reduces setup by a median of less than 1 cm (2B). The middle 95% of setup reduction due to vegetation (cm) is falls in the range [−5, 17]. Vegetation reduces runup by a median of 40 cm (3 B) and 90% (3C). The middle 95% of runup reduction due to vegetation

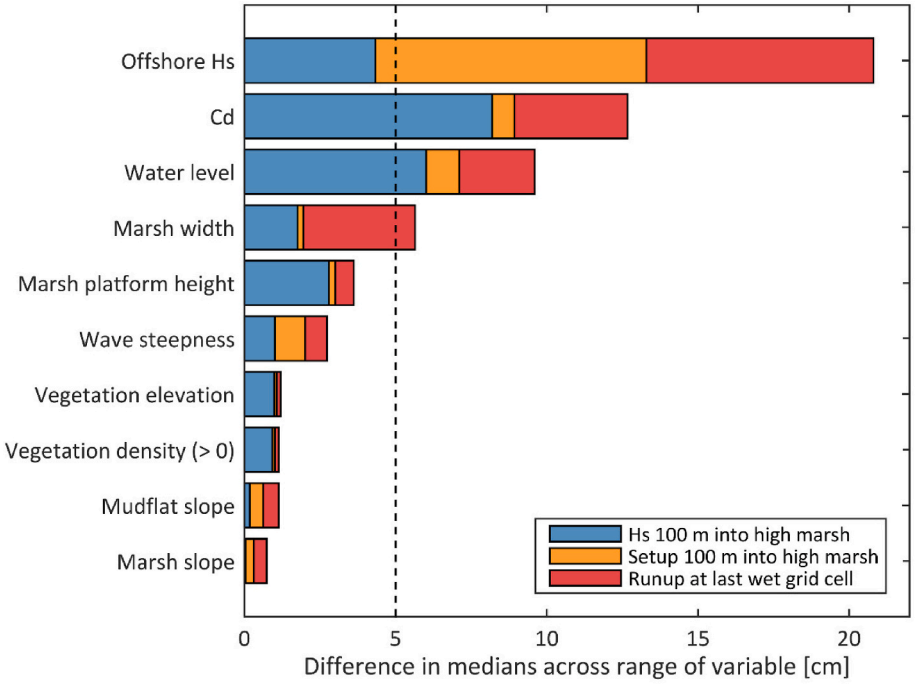

Fig. 8. The cumulative sum of the difference in medians of Hs, setup, and swash across the range of model settings used in 3.2. Variables which produced a cumulative sum greater than 5 cm, shown by the dashed line, were selected to be used in a subsequent analysis.

(cm) falls in the range [4, 133].

3.3.1. *Wave height*

The presence of vegetation plays a key role in reducing significant wave height in the marsh (Hs), shown by the empirical cumulative density plots in Fig. 10. When Cd = 0 (representing no vegetation), Hs increases for all model settings (1D). The widest spread in Hs reduction due to vegetation occurs with changes in wave height and water level (2B and 2C), meaning that vegetation is reducing Hs effectively across the range of water level and wave settings. Greatest values for Hs and Hs reduction by vegetation occur in simulations with largest waves (1B, 2B) and highest water levels (1C, 2C). Hs is highest with low Cd values (1D), and Hs reduction by vegetation is highest with high Cd values (2D). Wave steepness has limited effect wave height; marsh width also has limited effect because Hs is measured 100 m into the marsh, or at the last vegetated grid cell. Results show that vegetation reduces Hs by a median of 30 cm, and up to 118 cm even with the lowest friction coefficients (2D).

3.3.2. *Setup*

Vegetation influences setup through several mechanisms including radiation stress gradients (Buckley et al., 2016), wave-induced force due to emergent vegetation (Dean and Bender 2006), and wave-induced force due to skewed waves (Dean and Bender 2006), which each decrease setup; vegetation can also increase setup due to an increase in the mean drag force (Løvås and Tørum, 2001; Luhar et al., 2010). As a result, the influence of vegetation on setup is nuanced, as shown by the empirical cumulative density plots in Fig. 11. Extreme values for setup and setup reduction by vegetation occur in simulations wth largest waves (1B, 2B) and lowest water levels (1C, 2C). Narrow marshes (1E), no vegetation (1D), and the least steep waves (1A) result in highest values of setup. Setup reduction due to vegetation is greatest across wider marshes (2E) with higher Cd (2D); wave steepness has limited effect. The widest spread in setup reduction due to vegetation occurs with changes in water level. At lower water level settings, vegetation can reduce setup by more than 25 cm, while at higher water level settings, vegetation can increase setup by more than 5 cm (2C), likely due to large mean drag forces acting to increase setup in these settings (Løvås and Tørum, 2001; Luhar et al., 2010). Wave height also plays an important role, with vegetation resulting in the most significant increases and decreases in setup under the largest wave settings (2B).

3.3.3. *Runup*

Results show that the presence of vegetation plays a key role in reducing runup (setup + swash) across the range of simulation settings, shown by the empirical cumulative density plots in Fig. 12. Extreme values for runup and runup reduction by vegetation occur in simulations with largest waves (1B, 2B) and highest water levels (1C, 2C). Runup is highest with low Cd (1D) and runup reduction is highest with high Cd (2D). Runup is greatest across narrow mashes (1E), but vegetation reduces runup effectively even in the narrowest marshes (2E). Wave steepness has limited effect on runup and runup reduction due to vegetation. Results show that vegetation reduces runup by a median of 45 cm in the narrowest marshes (dark purple line in 2E) and by a median of 30 cm with the lowest friction coefficients (blue line in 2D). In both settings, vegetation can reduce runup by more than 130 cm.

3.4. *Extreme events*

In many locations in San Francisco Bay, marsh width is constrained between open water and levees. To understand the interplay between vegetation, marsh width, and extreme storm conditions, we explored the effects of marsh vegetation and marsh width in conditions representative of a present-day strong storm with wave heights of 1.5 m (O'Neill et al., 2017) and water level 1.15 m above MHHW (Nederhoff et al., 2021), or 3 m NAVD88, with wave steepness and Cd varied across the ranges shown in Table 3.

Results show that even in the narrowest marshes simulated (50 m), runup (setup + swash) is unlikely to exceed 25 cm, and that vegetation can reduce runup by a median of 65 cm across a 50 m marsh in storm conditions (Fig. 13). As marsh width increases, runup quickly decreases. Beyond 250 m of marsh width, additional width has limited impact on runup. Vegetation reduces runup most in narrower marsh settings because runup in unvegetated transects is greatest in narrower settings.

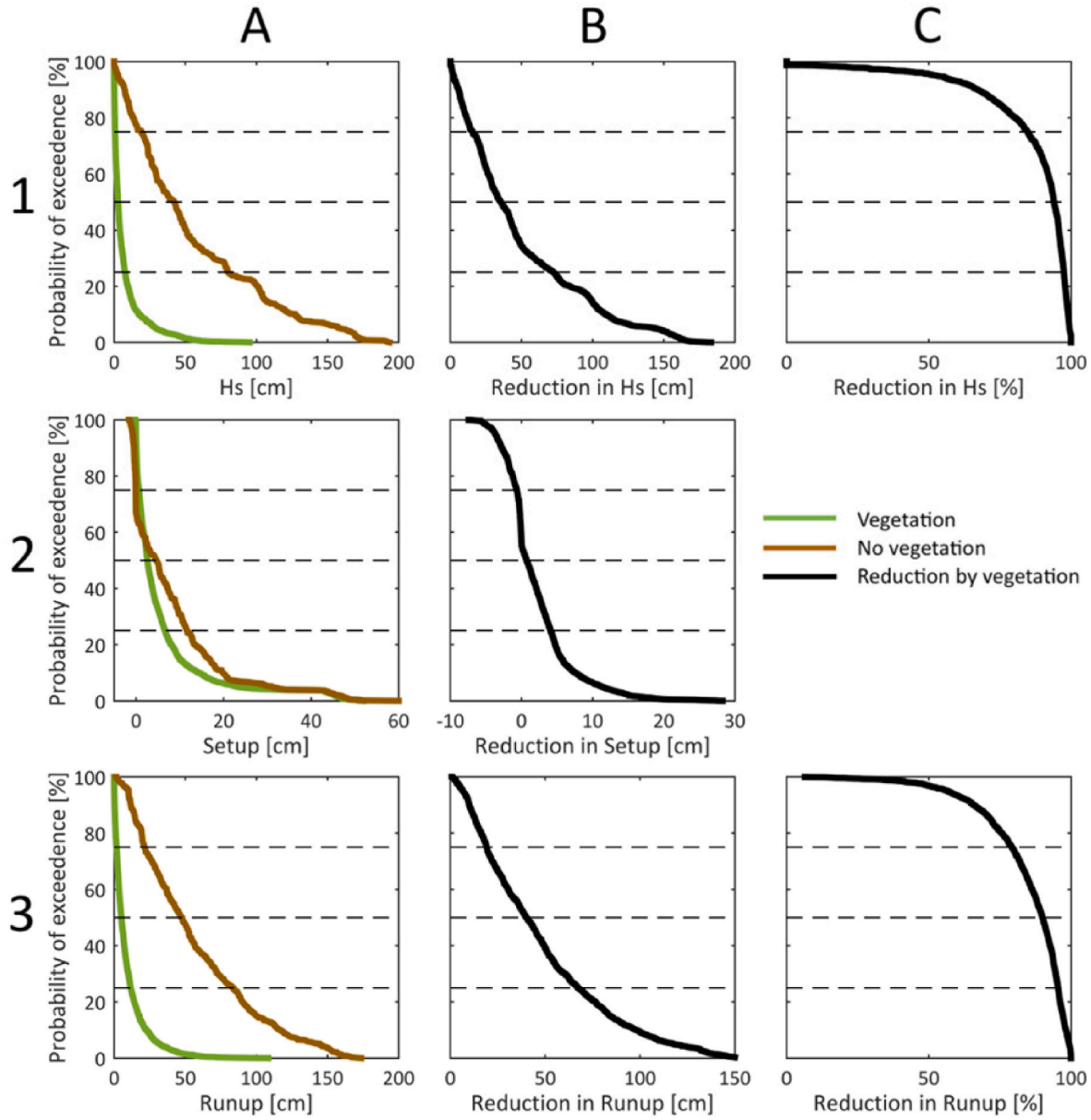

Fig. 9. An overview of results from the second round of simulations (n = 5^5) in which wave height, wave steepness, water level, drag coefficient (Cd), and marsh width were all covaried across the ranges identified in Table 3 and in which simulations were completed with and without vegetation. In column A, an empirical cumulative density function of significant wave height 100 m into the high marsh (Hs, row 1), setup 100 m into the high marsh (row 2), and runup at the last wet grid cell (row 3) with vegetation present (green) and vegetation removed (brown) from the transect. In column B and C, reduction in wave height 100 m into the high marsh (Hs, row 1), setup 100 m into the high marsh (row 2), and runup at the last wet grid cell (row 3) between vegetated and unvegetated transects, with absolute reduction in B, and percent reduction in C. Dotted lines show the 25th, 50th, and 75th percentiles. Across the range of settings explored here, vegetation reduces significant wave height 100 m into the marsh by a median of 35 cm (1 B); vegetation reduces setup by a median of less than 1 cm (2 B); and vegetation reduces runup by a median of 40 cm (3 B).

In the same hydrodynamic conditions representative of an extreme storm, across the range of marsh widths, Cd values, and wave steepness settings explored in this work, the main role vegetation plays in reducing nearshore water levels is through reducing swash. Vegetation reduces water levels at the base of the levee by a median of 55 cm primarily through reduction in swash (Fig. 14).

4. Discussion and conclusions

Vegetation on marshes can be effective in reducing potential wave induced flooding. In the range of model settings explored here, vegetation on a marsh reduces significant wave height by a median of 35 cm, causes minor changes in wave-induced setup (<5 cm), and reduces runup by a median of 40 cm (Fig. 9). Meaningful reductions in wave height and runup can be achieved even in the narrowest marshes simulated (50 m, Fig. 13).

Flood managers can use the information presented here to strategically plan for extreme events. For example, under conditions similar to a 100-year storm in San Francisco Bay, with offshore water level of 1.15 m above MHHW and wave heights of 1.5 m, 50 m of marsh vegetation reduces runup by a median of 65 cm and runup after a 50 m wide marsh will likely be less than 25 cm, reduced from as high as 1 m (Fig. 13). Under these same conditions, the dynamic water level at the base of the levee without vegetation is a median of 55 cm higher than it is with vegetation (Fig. 14), increasing likelihood of levee overtopping. High velocities introduced by wave overtopping of levees can introduce

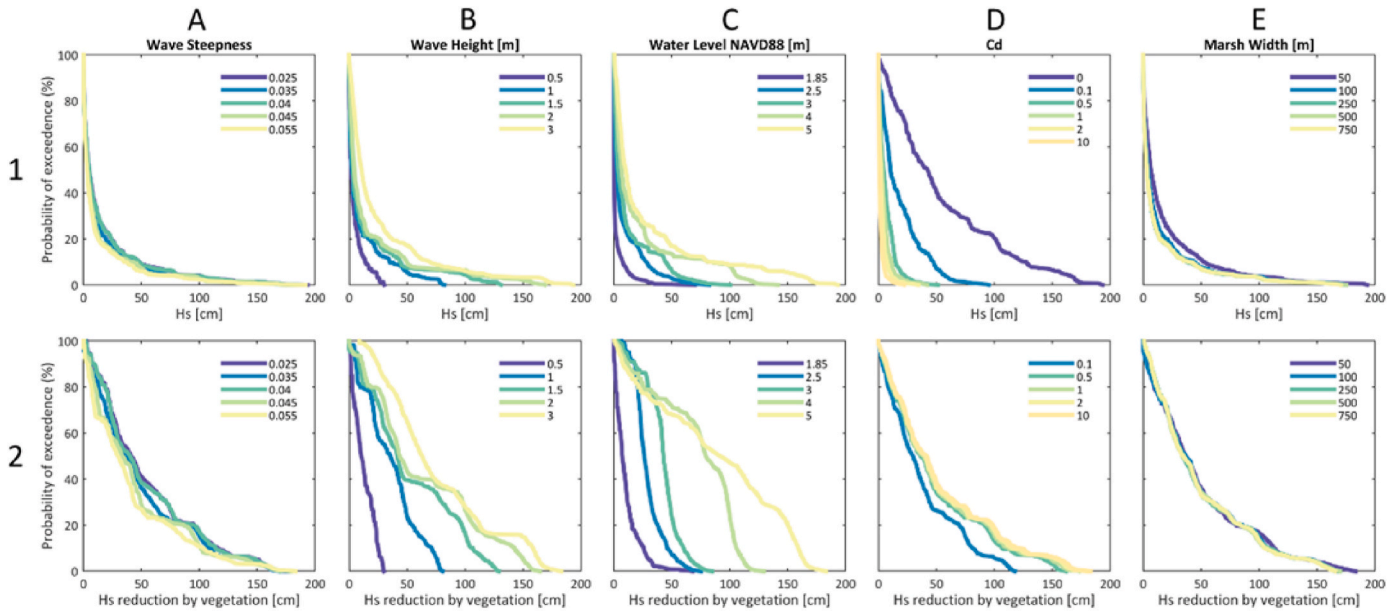

Fig. 10. In row 1, empirical cumulative density functions showing significant wave height 100 m into the high marsh; and in row 2, empirical density functions showing wave height reduction due to vegetation. Plots are separated from left to right by wave steepness (column A), wave height [m] (column B), water level [m NAVD88] (column C), drag coefficient (Cd) of vegetation (column D), and marsh width [m] (column E), with each single line on each subplot showing an empirical cumulative density function of the mean Hs values from 5^4 simulations. Results show that the presence of vegetation plays a key role in reducing wave height across the range of simulation settings.

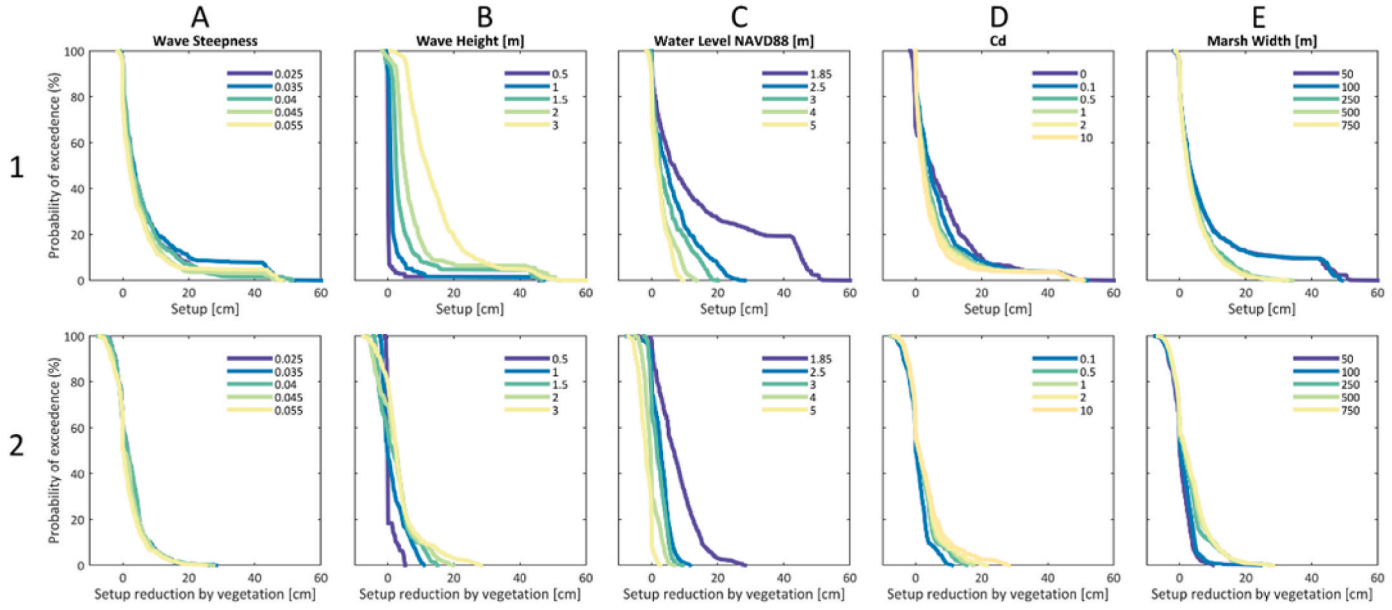

Fig. 11. In row 1, empirical cumulative density functions showing setup 100 m into the high marsh; and in row 2, empirical density functions showing setup reduction due to vegetation. Plots are separated from left to right by wave steepness (column A), wave height [m] (column B), water level [m NAVD88] (column C), drag coefficient (Cd) of vegetation (column D), and marsh width [m] (column E), with each single line on each subplot showing an empirical cumulative density function of the mean setup values from 5^4 simulations. Results show that the presence of vegetation plays a key role in influencing setup, particularly in low water level and in large wave settings.

turbulence, scouring, and erosion of levees, as modeled by Xiao et al. (2009) and observed during Hurricane Katrina in New Orleans, Louisiana, USA.

The validation presented here shows that the XB-NH model is capable of accurately simulating wave transformation of incident-band waves due to vegetation, allowing a first look at the effects of vegetation on incident-band driven runup. This has been achieved by utilizing a constant bulk drag coefficient (Cd) similar to other authors (van Rooijen et al., 2016) in which vegetation is schematized as a rigid-cylinder concept. Over the past several decades, several authors (Mendez and Losada, 2004; Pinsky et al., 2013; Jadhav et al., 2013; Möller et al., 2014; Foster-Martinez et al., 2018) have developed formulas to describe the relationship between Cd and Reynolds number (Re). The trend in these relationships is clear and shows that Cd decreases as conditions become more turbulent, with high Re. However, the specific relation varies widely between vegetation types and even

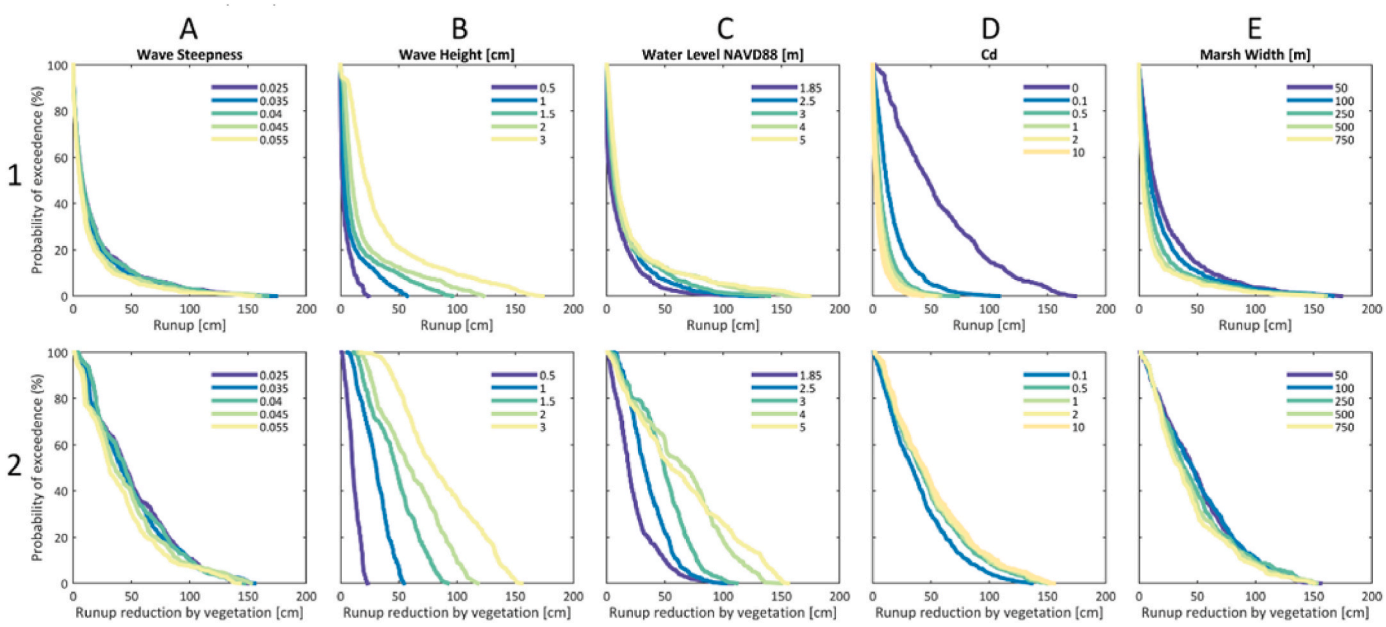

Fig. 12. In row 1, empirical cumulative density functions showing runup at the last wet grid cell; and in row 2, empirical density functions showing runup reduction due to vegetation. Plots are separated from left to right by wave steepness (column A), wave height [m] (column B), water level [m NAVD88] (column C), drag coefficient (Cd) of vegetation (column D), and marsh width [m] (column E) with each single line on each subplot showing an empirical cumulative density function of the mean runup values from 5^4 simulations. Results show that the presence of vegetation plays a key role in reducing runup across the range of simulation settings.

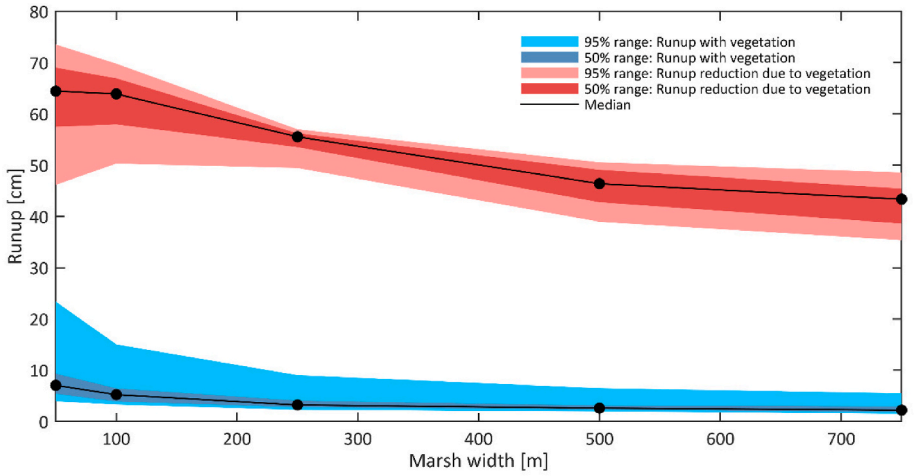

Fig. 13. Runup across a vegetated marsh (blue) and runup reduction due to vegetation (red) on the y axis, and marsh width on the x axis. Black dots show simulated marsh widths. Conditions represent an extreme storm in San Francisco Bay (wave height of 1.5 m and water level 1.15 m above MHHW).

between different studies of the same vegetation species. Pinsky et al. (2013) uniformly re-analyzed existing wave attenuation in marshes from 14 prior studies to determine a generalized relationship between Cd and Re. However, Cd is inherently difficult to measure, and is typically calculated using other vegetation measurements including stem height, stem density, and stem diameter, which each pose challenges in measurement due to seasonal, site, and species variability. These challenges have spurred recent developments in quantifying wave attenuation in marshes by their standing biomass rather than the parameters listed above (Maza et al., 2022), though this approach is not yet incorporated into numerical models like XBeach. Here, we utilized a constant Cd, determined from field measurements taken by Foster-Martinez et al. (2018) and varied it across three orders of magnitude. While we did not vary Cd as a function of Reynolds number in this study, 77% of hydrodynamic and Cd combinations fell within one standard deviation of the relationship derived by Pinsky et al. (2013), which is specific to marsh habitat; 13% fell below and 10% fell above one standard deviation. This is largely due to the high degree of uncertainty in relationships between Cd and Re, particularly beyond $Re > 10^3$, which is the upper limit of established relationships between Re and Cd. The uncertainty of our experimental simulations increases outside the calibrated range, but similarly to van Rooijen et al. (2016), our results show a relatively low sensitivity to a three order-of-magnitude variation in Cd in comparison to changes in hydrodynamics, as shown by the spread of empirical density curves in column D of Figs. 10–12. Further, based on the Pinsky et al. (2013) equation, a three order of magnitude variation in Cd is approximately the range expected for the range of Reynolds numbers simulated here. This is encouraging for applications in which vegetation measurements are limited and the vegetation bulk drag coefficient is unknown. The inverse relationship between Cd and Re results in outliers shown throughout Figs. 5–7, which occur with coincidence of high water-levels and low Cd. These simulations give insight to how wave

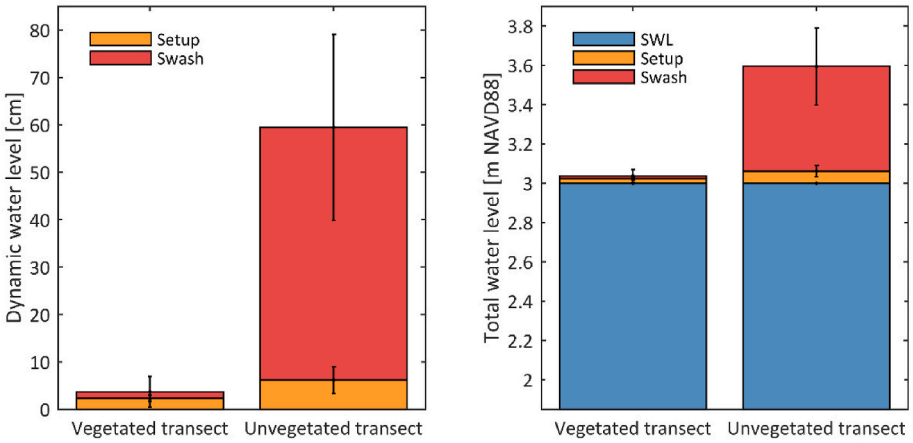

Fig. 14. Bar graphs showing components of the dynamic water level (left) and the total water level (right), with and without vegetation. Components of the dynamic water level include setup (measured 100 m into the marsh or at the last vegetated grid cell) and swash (measured at the last wet grid cell), and components of the total water level include the still water level (SWL), setup, and swash. The total water level y axis starts at the MHHW level. Bars represent median values and error bars show the middle 50% of values for setup and swash. Vegetation reduces the dynamic water level by a median of 55 cm in conditions representative of a present-day extreme storm (wave heights of 1.5 m and water level 1.15 m above MHHW), across a range of drag coefficient (Cd), marsh width, and wave steepness values.

transformation capacity of vegetated marshes may change in high water level settings due to changes in wave Reynolds number, driven by an increase in orbital velocity. To further explore how marsh plants can reduce wave driven flooding, we recommend prioritizing additional observational studies measuring wave attenuation in marshes, particularly during extreme hydrodynamic conditions, such as strong storms and high tides.

As sea levels rise, marshes may either vertically accrete, retreat landward, erode, or drown; the response of a marsh depends on sediment supply, location, and morphology. This study has parameterized these responses: a marsh accreting vertically gains marsh platform elevation (Fig. 7, column A); a marsh retreating increases the elevation where vegetation begins (Fig. 6, column C); a marsh laterally eroding steepens the low marsh slope (Fig. 7, column B); a marsh that drowns and transitions to mudflat loses vegetation density (Fig. 6, column A). Results from this study show that flood risk increases most drastically for marshes that lose vegetation density and transition to mudflat (Fig. 6, column A). In a setting similar to China Camp, transition to mudflat could mean increases of 50 cm in wave height at the marsh interior and increases of 30 cm in vertical wave runup (Fig. 6, A1, and A3, respectively), emphasizing the importance of maintaining marsh vegetation coverage in urban estuaries. In marshes that are providing important flood reduction services, managers could consider sediment nourishment to facilitate vegetation persistence with rising water level (Ganju 2019).

This work highlights the importance of continuing research on sediment dynamics in marshes and marsh response to higher water levels. Radioisotope dated cores show San Francisco Bay marshes have been keeping up with sea level rise over the last 150 years, with typical vertical accretion rates of 0.2–0.5 cm/year (Callaway et al., 2012). However, studies accounting for future sea level rise rates and current marsh accretion rates show that accretion rates are presently less than 4% of what will be necessary to keep up with accelerating sea level rise by the end of the 21st century (Knowles 2010; Barnard et al., 2013). The relative elevations of marshes in San Francisco Bay are predicted to decrease by 0.4–1.3 m by 2 100 (Swanson et al., 2014), causing marshes that do not have migration space to transition to mudflats (Elmilady et al., 2019).

Beyond San Francisco Bay, the majority of the world's megacities are coastal, and average global flood losses are expected to rise tenfold between 2005 and 2050, even with adaptation investments to maintain constant flood probability (Hallegatte et al., 2013). Many of these coastal megacities are at least partially protected by marshes, meaning that flood risk will be further amplified beyond SLR if marsh sedimentation rates are outpaced by SLR. Without rigorous sediment nourishment, there may be a tipping point after which relative elevations of marshes have decreased such that marsh habitat is not an effective flood defense. At that point, flood managers interested in nature-based shorelines could instead focus efforts on approaches such as vegetated levees to reduce swash, which still provide wave and flood reduction benefits of vegetation fields but are less sensitive to relative sea level.

Author contributions

Rae Taylor-Burns: conceptualization, methodology, software, validation, writing – original draft, writing – review & editing, funding acquisition. **Kees Nederhoff:** conceptualization, methodology, software, validation, writing – review & editing. **Jessica Lacy:** resources, data curation, writing – review & editing. **Patrick Barnard:** supervision, funding acquisition, writing – review & editing.

Any use of trade, firm, or product names is for descriptive purposes only and does not imply endorsement by the U.S. Government.

Declaration of competing interest

The authors declare that they have no known competing financial interests or personal relationships that could have appeared to influence the work reported in this paper.

Data availability

Data will be made available on request.

Acknowledgements

The authors would like to thank Maddie Foster-Martinez for sharing data and insights from the field campaign at China Camp. Additionally, we'd like to thank Rachel Allen and two anonymous reviewers for providing thoughtful comments and suggestions which improved this work. This research was funded by a California Sea Grant Graduate Research Fellowship NA180AR4170073 and by the U.S. Geological Survey Grant/Cooperative Agreement G17AC00361. The funding sources had no involvement in study design, data management, writing, or submission.

Appendix A. Supplementary data

Supplementary data to this article can be found online at https://doi.org/10.1016/j.coastaleng.2023.104346.

References

Barnard, Patrick L., Schoellhamer, David H., Jaffe, Bruce E., McKee, Lester J., 2013. Sediment transport in the San Francisco Bay coastal system: an overview. Mar. Geol. 345, 3–17. https://doi.org/10.1016/j.margeo.2013.04.005.

Barnard, Patrick L., Erikson, Li H., Foxgrover, Amy C., Hart, Juliette A Finzi, Limber, Patrick, Neill, Andrea C.O., Van Ormondt, Maarten, et al., 2019. Dynamic flood modeling essential to assess the coastal impacts of climate change. Nature Scientific Reports 9. https://doi.org/10.1038/s41598-019-40742-z.

Best, S.N., Van der Wegen, M., Dijkstra, J., Willemsen, P.W.J.M., Borsje, B.W., Roelvink, Dano J.A., 2018. Do salt marshes survive sea level rise? Modelling wave action, morphodynamics and vegetation dynamics. Environ. Model. Software 109, 152–166. https://doi.org/10.1016/j.envsoft.2018.08.004.

Bigalbal, Alayna, Rezaie, Ali M., Garzon, Juan L., Ferreira, Celso M., 2018. Potential impacts of sea level rise and coarse scale marsh migration on storm surge hydrodynamics and waves on coastal protected areas in the Chesapeake Bay. Marine Science and Engineering 6. https://doi.org/10.3390/jmse6030086.

Bouma, T.J., Temmerman, S., van Duren, L.A., Martini, E., Vandenbruwaene, W., Callaghan, D.P., Balke, T., et al., 2013. Organism traits determine the strength of scale-dependent bio-geomorphic feedbacks: a flume study on three intertidal plant species. Geomorphology 180–181, 57–65. https://doi.org/10.1016/j.geomorph.2012.09.005.

Buckley, Mark L., Lowe, Ryan J., Hansen, Jeff E., Van Dongeren, Ap R., 2016. Wave setup over a fringing reef with large bottom roughness. J. Phys. Oceanogr. 46 (8), 2317–2333. https://doi.org/10.1175/JPO-D-15-0148.1.

Buffington, K.J., Thorne, K.M., 2018. LEAN-corrected San Francisco Bay Digital Elevation Model." U.S. Geological Survey.

Callaghan, D.P., Bouma, T.J., Klaassen, P., van der Wal, D., Stive, M.J.F., Herman, P.M.J., 2010. Hydrodynamic forcing on salt-marsh development: distinguishing the relative importance of waves and tidal flows. Estuar. Coast Shelf Sci. 89 (1), 73–88. https://doi.org/10.1016/j.ecss.2010.05.013.

Callaway, John C., Borgnis, Evyan L., Turner, R. Eugene, Milan, Charles S., 2012. Carbon sequestration and sediment accretion in San Francisco Bay tidal wetlands. Estuar. Coast 35 (5), 1163–1181. https://doi.org/10.1007/s12237-012-9508-9.

Chow, Ven Te, 1959. Open-Channel Hydraulics. McGraw-Hill Book Company, Inc.

Dalrymple, Robert A., ASCE, M., Kirby, James T., Hwang, Paul A., 1984. Wave diffraction due to areas of energy dissipation. J. Waterw. Port, Coast. Ocean Eng. 110 (1), 67–79.

Danielson, Jeffrey J., Poppenga, Sandra K., Brock, John C., Evans, Gayla A., Tyler, Dean J., Gesch, Dean B., Thatcher, Cindy A., Baras, John A., 2016. Topobathymetric elevation model development using a new methodology : coastal national elevation database. J. Coast Res. 76 https://doi.org/10.2112/SI76-008.

de Ridder, Menno P., Smit, Pieter B., van Dongeren, Ap, McCall, Robert, Nederhoff, Kees, Reniers, Ad J.H.M., 2020. Efficient two-layer non-hydrostatic wave model with accurate dispersive behaviour. Coast. Eng. 164, 103808 https://doi.org/10.1016/j.coastaleng.2020.103808.

Dean, Robert G., Bender, Christopher J., 2006. Static wave setup with emphasis on damping effects by vegetation and bottom friction. Coast. Eng. 53 (2–3), 149–156. https://doi.org/10.1016/j.coastaleng.2005.10.005.

DeConto, Robert M., Pollard, David, 2016. Contribution of Antarctica to past and future sea-level rise. Nature 531 (7596), 591–597. https://doi.org/10.1038/nature17145.

Desmond, J., Williams, G., James, M., Johnson, J., Callaway, J., Zedler, J., 1999. Tijuana River National Estuarine Research Reserve: Annual Report on Ecosystem Monitoring. Pacific Estuarine Research Laboratory, San Diego, California.

Ellison, A.M., 1987. Effects of competition, disturbance, and herbivory on Salicornia europaea. Ecology. https://doi.org/10.2307/1938463.

Elmilady, H., van der Wegen, M., Roelvink, D., Jaffe, B.E., 2019. Intertidal area disappears under sea level rise: 250 Years of morphodynamic modeling in San Pablo Bay, California. J. Geophys. Res.: Earth Surf. 124 (1), 38–59. https://doi.org/10.1029/2018JF004857.

Fernandes, Elisa Helena, Dyer, Keith Richard, Luis Felipe Hax, Niencheski, 2000. Calibration and validation of the TELEMAC-2D model to the Patos Lagoon (Brazil). J. Coast Res. 470–488.

Foster-Martinez, M.R., Lacy, J.R., Ferner, M.C., Variano, E.A., 2018. Wave attenuation across a tidal marsh in San Francisco Bay. Coast. Eng. 136, 26–40. https://doi.org/10.1016/j.coastaleng.2018.02.001.

Ganju, Neil K., 2019. Marshes are the new beaches: integrating sediment transport into restoration planning. Estuar. Coast 42 (4), 917–926. https://doi.org/10.1007/s12237-019-00531-3.

Garzon, Juan L., Maza, M., Ferreira, C.M., Lara, J.L., Losada, I.J., 2019. Wave attenuation by Spartina saltmarshes in the Chesapeake Bay under storm surge conditions. J. Geophys. Res.: Oceans 124 (7), 5220–5243. https://doi.org/10.1029/2018JC014865.

Gittman, Rachel K., Popowich, Alyssa M., Bruno, John F., Peterson, Charles H., 2014. Marshes with and without sills protect estuarine shorelines from erosion better than bulkheads during a category 1 Hurricane. Ocean Coast Manag. 102, 94–102. https://doi.org/10.1016/j.ocecoaman.2014.09.016.

Guza, R.T., Thornton, E.B., 1981. Wave set-up on a natural beach. J. Geophys. Res. 86 (C5), 4133–4137. https://doi.org/10.1029/JC086iC05p04133.

Guza, R.T., Thornton, E.B., 1982. Swash oscillations on a natural beach. J. Geophys. Res. 87 (C1), 483–491. https://doi.org/10.1029/JC087iC01p00483.

Guza, R.T., Thornton, E.B., Holman, R.A., 1984. Swash on steep and shallow beaches. Proceedings of the Nineteenth International Conference on Coastal Engineering 708. https://doi.org/10.9753/icce.v19.48, 23.

Hallegatte, Stephane, Green, Colin, Nicholls, Robert, J., Corfee-Morlot, Jan, 2013. Future flood losses in major coastal cities. Nat. Clim. Change 3 (9), 802–806. https://doi.org/10.1038/nclimate1979.

Harris, Daniel L., Rovere, Alessio, Casella, Elisa, Power, Hannah, Canavesio, Remy, Antoine, Collin, Pomeroy, Andrew, Webster, Jody M., Parravicini, Valeriano, 2018. Coral reef structural complexity provides important coastal protection from waves under rising sea levels. Sci. Adv. 4 (2), 1–8. https://doi.org/10.1126/sciadv.aao4350.

Hasselmann, K., 1974. On the spectral dissipation of ocean waves due to white capping. Boundary-Layer Meteorol. 6, 107–127.

Hasselmann, K., Barnett, T.P., Bouws, E., Carlson, H., Cartwright, D.E., Enke, K., Ewing, J.A., et al., 1973. Measurements of Wind-Wave Growth and Swell Decay during the Joint North Sea Wave Project (JONSWAP).

Jadhav, Ranjit S., Chen, Qin, Smith, Jane M., 2013. Spectral distribution of wave energy dissipation by salt marsh vegetation. Coast. Eng. 77, 99–107. https://doi.org/10.1016/j.coastaleng.2013.02.013.

Karimpour, Arash, Chen, Qin, Twilley, Robert R., 2017. Wind wave behavior in fetch and depth limited estuaries. Sci. Rep. 7, 1–8. https://doi.org/10.1038/srep40654. December 2016.

Kimmerer, Wim J., 2004. Open water processes of the San Francisco estuary: from physical forcing to biological responses. San Franc. Estuary Watershed Sci. 2 (1) https://doi.org/10.15447/sfews.2004v2iss1art1.

Kirwan, Matthew L., Guntenspergen, Glenn R., D'Alpaos, Andrea, Morris, James T., Mudd, Simon M., Temmerman, Stijn, 2010. Limits on the adaptability of coastal marshes to rising sea level. Geophys. Res. Lett. 37 (23), 1–5. https://doi.org/10.1029/2010GL045489.

Knowles, Noah, 2010. Potential inundation due to rising sea levels in the San Francisco Bay region. San Franc. Estuary Watershed Sci. 8 (1) https://doi.org/10.15447/sfews.2010v8iss1art1.

Lacy, J.R., Allen, R.M., Foster-Martinez, M.R., Ferreira, J.C.. O'Neill, A.C, 2017. Hydrodynamic and sediment transport data from San Pablo Bay and China Camp marsh (northern San Francisco Bay). https://doi.org/10.5066/F7HM56MX.

Lacy, Jessica R., MacVean, Lissa J., 2016. Wave attenuation in the shallows of San Francisco bay. Coast. Eng. 114, 159–168. https://doi.org/10.1016/j.coastaleng.2016.03.008.

le Bars, Dewi, Drijfhout, Sybren, De Vries, Hylke, 2017. A high-end sea level rise probabilistic projection including rapid Antarctic ice sheet mass loss. Environ. Res. Lett. 12 (4) https://doi.org/10.1088/1748-9326/aa6512.

Longuet-Higgins, M.S., Stewart, R.W., 1963. A note on wave set-up. J. Mar. Res. 11 (2), 324. https://doi.org/10.1016/0011-7471(64)90258-x.

Løvås, Magnar Stig, Tørum, Alf, 2001. Effect of the kelp Laminaria hyperborea upon sand dune erosion and water particle velocities. Coast. Eng. 44 (1), 37–63. https://doi.org/10.1016/S0378-3839(01)00021-7.

Luhar, Mitul, Coutu, Sylvain, Infantes, Eduardo, Fox, Samantha, Nepf, Heidi, 2010. Wave-induced velocities inside a model seagrass bed. J. Geophys. Res.: Oceans 115 (12), 1–15. doi:10.1029/2010JC006345.

Ma, Gangfeng, Kirby, James T., Su, Shih Feng, Figlus, Jens, Shi, Fengyan, 2013. Numerical study of turbulence and wave damping induced by vegetation canopies. Coast. Eng. 80, 68–78. https://doi.org/10.1016/j.coastaleng.2013.05.007.

Masson-Delmotte, V., Zhai, P., Pirani, A., Connors, S.L., Péan, C., Berger, S., Caud, N., et al., 2021. "IPCC, 2021: summary for policymakers. In: Climate Change 2021: the Physical Science Basis. Contribution of Working Group I to the Sixth Assessment Report of the Intergovernmental Panel on Climate Change.". Cambridge University Press.

Maza, M., Lara, J.L., Losada, I.J., Ondiviela, B., Trinogga, J., Bouma, T.J., 2015. Large-scale 3-D experiments of wave and current interaction with real vegetation. Part 2: experimental analysis. Coast. Eng. 106, 73–86. https://doi.org/10.1016/j.coastaleng.2015.09.010.

Maza, Maria, Lara, Javier L., Losada, Iñigo J., 2022. A paradigm shift in the quantification of wave energy attenuation due to saltmarshes based on their standing biomass. Sci. Rep. 1–13. https://doi.org/10.1038/s41598-022-18143-6.

Mendez, Fernando J., Losada, Inigo J., 2004. An empirical model to estimate the propagation of random breaking and nonbreaking waves over vegetation fields. Coast. Eng. 51 (2), 103–118. https://doi.org/10.1016/j.coastaleng.2003.11.003.

Menéndez, Pelayo, Losada, Iñigo J., Torres-Ortega, Saul, Narayan, Siddharth, Beck, Michael W., 2020. The global flood protection benefits of mangroves. Sci. Rep. 10 (1), 1–11. https://doi.org/10.1038/s41598-020-61136-6.

Merkens, Jan-ludolf, Reimann, Lena, Hinkel, Jochen, Vafeidis, Athanasios T., 2016. Gridded population projections for the coastal zone under the shared socioeconomic pathways. Global Planet. Change 145, 57–66. https://doi.org/10.1016/j.gloplacha.2016.08.009.

Miche, M., 1951. Le Pouvoir Réfléchissant Des Ouvrages Maritimes Exposés à l'action de La Houle. Annales de Ponts et Chaussées 121, 285–319.

Möller, Iris, Kudella, Matthias, Rupprecht, Franziska, Spencer, Tom, Paul, Maike, Bregje, K., van Wesenbeeck, Guido, Wolters, et al., 2014. Wave attenuation over coastal salt marshes under storm surge conditions. Nat. Geosci. 7, 727–731.

Narayan, Siddharth, Beck, Michael W., Reguero, Borja G., Losada, Iñigo J., Van Wesenbeeck, Bregje, Pontee, Nigel, Sanchirico, James N., Carter Ingram, Jane, Marie Lange, Glenn, Burks-Copes, Kelly A., 2016. The effectiveness, costs and coastal protection benefits of natural and nature-based defences. PLoS One 11 (5), 1–17. https://doi.org/10.1371/journal.pone.0154735.

Narayan, Siddharth, Beck, Michael W., Wilson, Paul, Thomas, Christopher J., Guerrero, Alexandra, Shepard, Christine C., Reguero, Borja G., Franco, Guillermo, Carter Ingram, Jane, Trespalacios, Dania, 2017. The value of coastal wetlands for flood damage reduction in the northeastern USA. Sci. Rep. 7 (1), 1–12. https://doi.org/10.1038/s41598-017-09269-z.

Nederhoff, Kees, Rohin, Saleh, Tehranirad, Babak, Herdman, Liv, Li, Erikson, Barnard, Patrick L., van der Wegen, Mick, 2021. Drivers of Extreme Water Levels in a Large, Urban, High-Energy Coastal Estuary – A Case Study of the San Francisco Bay. Coastal Engineering.

Nowacki, Daniel J., Beudin, Alexis, Ganju, Neil K., 2017. Spectral wave dissipation by submerged aquatic vegetation in a back-barrier estuary. Limnol. Oceanogr. 62 (2), 736–753. https://doi.org/10.1002/lno.10456.

O'Neill, A.C., Erikson, L.H., Barnard, P.L., 2017. Downscaling wind and wavefields for 21st century coastal flood hazard projections in a region of complex terrain. Earth Space Sci. 4 (5), 314–334. https://doi.org/10.1002/2016EA000193.

Pinsky, Malin L., Guannel, Greg, Arkema, Katie K., 2013. Quantifying wave attenuation to inform coastal habitat conservation. Ecosphere 4 (8). https://doi.org/10.1890/ES13-00080.1.

Powell, Emily J., Tyrrell, Megan C., Milliken, Andrew, Tirpak, John M., Staudinger, Michelle D., 2019. A review of coastal management approaches to support the integration of ecological and human community planning for climate change. J. Coast Conserv. 23 (1), 1–18. https://doi.org/10.1007/s11852-018-0632-y.

Putnam, J.A., 1949. Loss of wave energy due to percolation in a permeable sea bottom. Trans. Am. Geophys. Union 30 (3).

Putnam, J.A., Johson, J.W., 1949. The Dissipation of Wave Energy by Bottom Friction. Transations, American Geophysical Union 30 (1).

Quataert, Ellen, Storlazzi, Curt, Arnold van Rooijen, Cheriton, Olivia, Dongeren, Ap, 2015. The influence of coral reefs and climate change on wave-driven flooding of tropical coastlines. https://doi.org/10.1002/2015GL064861, 42: 6407–15.

Ranasinghe, Roshanka, Trang Minh, Duong, Uhlenbrook, Stefan, Roelvink, Dano, Stive, Marcel, 2013. Climate-change impact assessment for inlet-interrupted coastlines. Nat. Clim. Change 3 (1), 83–87. https://doi.org/10.1038/nclimate1664.

Reguero, Borja, G., Storlazzi, Curt D., Gibbs, Ann E., Shope, James B., Cole, Aaron D., Cumming, Kristen A, Beck, Michael W., 2021. The value of U.S. coral reefs for flood risk reduction. Nat. Sustain. 4 (8), 688–698. https://doi.org/10.1038/s41893-021-00706-6.

Roelvink, Dano, McCall, Robert, Mehvar, Seyedabdolhossein, Nederhoff, Kees, Ali, Dastgheib, 2018. Improving predictions of swash dynamics in XBeach: the role of groupiness and incident-band runup. Coast. Eng. 134 (July 2017), 103. https://doi.org/10.1016/j.coastaleng.2017.07.004. –23.

Roelvink, Dano, Reniers, Ad, van Dongeren, Ap, Jaap van Thiel de Vries, McCall, Robert, Lescinski, Jamie, 2009. Modelling storm impacts on beaches, dunes and barrier islands. Coast. Eng. 56 (11–12), 1133–1152. https://doi.org/10.1016/j.coastaleng.2009.08.006.

Schile, Lisa M., Callaway, John C., Diana Stralberg, James T. Morris, Parker, V. Thomas, Kelly, Maggi, 2014. Modeling tidal marsh distribution with sea-level rise: evaluating the role of vegetation, sediment, and upland habitat in marsh resiliency. PLoS One 9 (2). https://doi.org/10.1371/journal.pone.0088760.

Shemdin, O., Hasselmann, K., Hsiao, S.V., Herterich, K., 1978. Nonlinear and linear bottom interaction effects in shallow water. In: Turbulent Fluxes through the Sea Surface, Wave Dynamics, and Prediction, 347–72. Plenum Press, New York. https://doi.org/10.1007/978-1-4612-9806-9_23.

Shen, Jian, Wang, Harry, Mac Sisson, Gong, Wenping, 2006. Storm tide simulation in the Chesapeake Bay using an unstructured grid model. Estuar. Coast Shelf Sci. 68 (1), 1–16. https://doi.org/10.1016/j.ecss.2005.12.018.

Shepard, Christine C., Crain, Caitlin M., Beck, Michael W., 2011. The protective role of coastal marshes: a systematic review and meta-analysis. PLoS One 6 (11). https://doi.org/10.1371/journal.pone.0027374.

Smit, Pieter, Zijlema, Marcel, Guus Stelling, 2013. Depth-induced wave breaking in a non-hydrostatic, near-shore wave model. Coast. Eng. 76, 1–16. https://doi.org/10.1016/j.coastaleng.2013.01.008.

Stockdon, Hilary F., Holman, Rob A., Howd, Peter A., Sallenger, Asbury H., 2006. Empirical parameterization of setup, swash, and runup. Coast. Eng. 53 (7), 573–588. https://doi.org/10.1016/j.coastaleng.2005.12.005.

Storlazzi, Curt D., Reguero, Borja G., Cole, Aaron D., Lowe, Erik, Shope, James B., Gibbs, Ann E., Nickel, Barry A., McCall, Robert T., van Dongeren, Ap R., Beck, Michael W., 2019. Rigorously valuing the role of U.S. coral reefs in coastal hazard risk reduction: U.S. Geological Survey Open File Report 2019-1027. https://doi.org/10.3133/ofr20191027.

Stralberg, Diana, Brennan, Matthew, Callaway, John C., Wood, Julian K., Schile, Lisa M., Jongsomjit, Dennis, Kelly, Maggi, Thomas Parker, V., Crooks, Stephen, 2011. Evaluating tidal marsh sustainability in the face of sea-level rise: a hybrid modeling approach applied to San Francisco Bay. PLoS One 6 (11). https://doi.org/10.1371/journal.pone.0027388.

Stutz, Matthew L., Sam Smith, A.W., Pilkey, Orrin H., 1998. Differing mechanisms of wave energy dissipation in the wave shoaling zone, surf zone and swash zone; why a uniform rate of wave energy dissipation is impossible; proceedings of the international coastal symposium (ICS98). In: International Coastal Symposium (ICS98), Palm Beach, FL, United States, May 19-23, 1998 Special Is (26), pp. 214–218.

Suzuki, Tomohiro, Zijlema, Marcel, Burger, Bastiaan, Meijer, Martijn C., Narayan, Siddharth, 2012. Wave dissipation by vegetation with layer schematization in SWAN. Coast. Eng. 59 (1), 64–71. https://doi.org/10.1016/J.COASTALENG.2011.07.006.

Swanson, Kathleen M., Drexler, Judith Z., Schoellhamer, David H., Thorne, Karen M., Casazza, Mike L., Overton, Cory T., Callaway, John C., Takekawa, John Y., 2014. Wetland accretion rate model of ecosystem resilience (WARMER) and its application to habitat sustainability for endangered species in the San Francisco Estuary. Estuar. Coast 37 (2), 476–492. https://doi.org/10.1007/s12237-013-9694-0.

Sweet, W.V., Kopp, R.E., Weaver, C.P., Obeysekera, J., Horton, R.M., Thieler, E.R., Zervas, Chris, 2017. "Global and regional sea level rise scenarios for the United States," no. NOS CO-OPS 083: 75. https://tidesandcurrents.noaa.gov/publications/techrpt83_Global_and_Regional_SLR_Scenarios_for_the_US_final.pdf.

Sweet, W.V., Hamlington, B.D., Kopp, R.E., Weaver, C.P., Barnard, P.L., Bekaert, D., Brooks, W., et al., 2022. Global and Regional Sea Level Rise Scenarios for the United States: Updated Mean Projections and Extreme Water Level Probabilities along U.S. Coastlines.

Taherkhani, Mohsen, Vitousek, Sean, Barnard, Patrick L., Frazer, Neil, Anderson, Tiffany R., Fletcher, Charles H., 2020. Sea-level rise exponentially increases coastal flood frequency. Sci. Rep. 10 (1), 1–18. https://doi.org/10.1038/s41598-020-62188-4.

Takekawa, J.Y., Thorne, K.M., Buffington, K.J., Spragens, K.A., Swanson, K.M., Drexler, J.Z., Schoellhamer, D.H., Overton, C.T., Casazza, M.L., 2013. Final Report for Sea-Level Rise Response Modeling for San Francisco Bay Estuary Tidal Marshes." U.S. Geological Survey Open File Report.

Talke, S.A., Stacey, M.T., 2003. The influence of oceanic swell on flows over an estuarine intertidal mudflat in San Francisco Bay. Estuar. Coast Shelf Sci. 58 (3), 541–554. https://doi.org/10.1016/S0272-7714(03)00132-X.

Tommasini, Laura, Carniello, Luca, Ghinassi, Massimiliano, Roner, Marcella, D'Alpaos, Andrea, 2019. Changes in the wind-wave field and related salt-marsh lateral erosion: inferences from the evolution of the Venice Lagoon in the last four centuries. Earth Surf. Process. Landforms 44 (8), 1633–1646. https://doi.org/10.1002/esp.4599.

van Rooijen, A.A., McCall, R.T., van Thiel de Vries, J.S.M., van Dongeren, A.R., Reniers, A.J.H.M., Roelvink, J.A., 2016. Modeling the effect of wave vegetation interaction on wave setup. J. Geophys. Res.: Oceans 121. https://doi.org/10.1002/2015JC011486.Received.

van Rooijen, A.A., van Thiel de Vries, J.S.M., McCall, R.T., van Dongeren, A.R., Roelvink, J.A., Reniers, A.J.H.M., 2015. Modeling of wave attenuation by vegetation with XBeach. E-Proceedings of the 36th IAHR World Congress 7.

van Zelst, Vincent T.M., Dijkstra, Jasper T., van Wesenbeeck, Bregje K., Eilander, Dirk, Morris, Edward P., Winsemius, Hessel C., Ward, Philip J., de Vries, Mindert B., 2021. Cutting the costs of coastal protection by integrating vegetation in flood defences. Nat. Commun. 12 (1), 1–11. https://doi.org/10.1038/s41467-021-26887-4.

Vitousek, Sean, Barnard, Patrick L., Fletcher, Charles H., Frazer, Neil, Erikson, Li H., Storlazzi, Curt D., 2017. Doubling of coastal flooding frequency within decades due to sea-level rise. Sci. Rep. 7, 1–9. https://doi.org/10.1038/s41598-017-01362-7.

Ward, Kristen M., Callaway, John C., Zedler, Joy B., 2003. Episodic colonization of an intertidal mudflat by native cordgrass (Spartina foliosa) at Tijuana Estuary. Estuaries 26 (1), 116–130. https://doi.org/10.1007/BF02691699.

Wesenbeeck, Bregje K. van, Guido, Wolters, Antolínez, José A.A., Kalloe, Sudarshini A., Hofland, Bas, Wiebe, P., de Boer, Çete, Ceylan, Bouma, Tjeerd J., 2022. Wave attenuation through forests under extreme conditions. Sci. Rep. 12 (1), 1–8. https://doi.org/10.1038/s41598-022-05753-3.

Woo, I., Takekawa, J.Y., 2012. Will inundation and salinity levels associated with projected sea level rise reduce the survival, growth, and reproductive capacity of Sarcocornia pacifica (pickleweed)? Aquatic Botany 102, 8–14. https://doi.org/10.1016/j.aquabot.2012.03.014.

Wright, L.D., Short, A.D., 1984. Morphodynamic variability of surf zones and beaches: a synthesis. Mar. Geol. 56 (1–4), 93–118. https://doi.org/10.1016/0025-3227(84)90008-2.

Xiao, Hong, Huang, Wenrui, Tao, Jianhua, 2009. Numerical modeling of wave overtopping a levee during Hurricane Katrina. Comput. Fluid 38 (5), 991–996. https://doi.org/10.1016/j.compfluid.2008.01.025.

Ysebaert, Tom, Yang, Shi Lun, Zhang, Liquan, He, Qing, Bouma, Tjeerd J., Herman, Peter M.J., 2011. Wave attenuation by two contrasting ecosystem engineering salt marsh macrophytes in the intertidal pioneer zone. Wetlands 31 (6), 1043–1054. https://doi.org/10.1007/s13157-011-0240-1.

Zhao, Dongliang, Li, Moxin, 2019. Dependence of wind stress across an air–sea interface on wave states. J. Oceanogr. 75 (3), 207–223. https://doi.org/10.1007/s10872-018-0494-9.

Zijlema, Marcel, Guus Stelling, Smit, Pieter, 2011. SWASH: an operational public domain code for simulating wave fields and rapidly varied flows in coastal waters. Coast. Eng. 58 (10), 992–1012. https://doi.org/10.1016/j.coastaleng.2011.05.015.